Altahadi University
Faculty of Engineering
Electrical Engineering Department

Sand and Dust Storms Effects on Microwave links, Case study Agedabia -to- Jalo .

Submitted by:
Hassan Abdallah Aldeeb

Supervised by:
Dr. Sayeh Mohamed Elhabashi

As partial fulfillment of the requirement for Master of Science degree

Spring 2007

Sirte – Libya

Altahadi University
Faculty of Engineering
Department of Electrical Engineering

M. Sc. Thesis Title :

Sand and Dust Storms Effects on Microwave links, Case study Agedabia-to- Jalo .

Prepared by:

Hassan Abdallah Aldeeb

Approved by:

Supervisor	Dr. Sayeh M. Elhabashi	Signature:
Internal examiner	Dr.Ahmed M. Gallai	Signature:
External examiner	Dr. Ibrahim M. Saleh	Signature:

Spring 2007

Sirte – Libya

جامعة التحدى – سرت
كلية الهندسة
قسم الهندسة الكهربائية

رسالة الماجستير

تأثير العواصف الرملية والغبار على وصلات الميكروويف بين منطقتى إجدابيا وجالو

إعداد : حسن عبدالله الديب

لجنة المناقشة

المشرف : د. السائح محمد الهباشى التوقيع :.....

الممتحن الداخلى : د. أحمد محمد القلاى التوقيع .....

الممتحن الخارجى : د. ابراهيم محمد صالح التوقيع :.....

ربيع 2007 ف
سرت – ليبيا

ABSTRACT

The aim of this thesis is to study the effect of dust and sand storms on the microwave links and apply the results of this study to the microwave link from Agedabia to Jalo between longitude (20.13 to 21.40 N) and latitude (30.45 to 29.10 E) .

The first step is the collection of dust and sand samples from seven sites from Agedabia to Jalo and analyze them to find the chemical composition and practical size distribution PSD.

The second step is it find the relative permittivity and calculate the visibility from the wind speed data and the results of step one.

The third step is to calculate the attenuation factor and from it find the attenuation to the wave for the path that has the longest distance in the region under the study.

الملخص

الهدف من هذا المشروع دراسة تأثير العواصف الرملية والغبارية على وصلات الميكروويف ، وتطبيق هذه الدراسة على منظومة الميكروويف الرابطة مابين مدينتي إجدابيا وجالو واللتان تقعان في المنطقة المحصورة بين خطي طول (20.13 الى 21.40 شمالا) وخطى عرض (30.45 الى 29.10 شرقاً) .

الخطوة الأولي تتمثل في تجميع عينات الرمل والغبار من سبع مواقع مختلفة وإيجاد التركيب الكيميائي وأبعاد جزيئاتها . والخطوة الثانية هي استخدام نتائج هذه التحاليل في إيجاد النفاذية الكهربائية النسبية لهذه العينات (ϵ_r) ، وتحديد معدل الرؤية أثناء العواصف بمنطقة الدراسة.

الخطوة الثالثة تتمثل في حساب معامل التوهين (α) الذي يسببه الغبار والعواصف الرملية على منظومات الميكروويف . لنستنتج منها مدى التأثير الذي تسببه هذه العواصف على منظومة الميكروويف لمنطقة الدراسة .

الإهـــــداء

إلى من لو جئت بكلام الدنيا كله لما وفيتهم حقهم

ولولا دعاؤهم لي بعد الله تعالى لما وصلت لما أنا عليه الآن

أمي وأبي

إلى من عانت ورافقت معي طيلة أيام دراستي وتحملت معي الكثير،

زوجتي الغالية

إلى أغلى ما لدي في هذا الوجود وقرة عيني

إبني الغاليين سيف الإسلام وعبد الله

إلى من أشد بهم أزري وسندي واعتز بهم

إخوتي وأخواتي

إلى كل أقاربي من أبناء عمي وأخوالي الذين ترتفع بهم هامتي

إلى كل الأصدقاء الذين ما فتئوا يشدون من أزري لإنهاء دراستي

إلى أساتذتي الذين هم زادي العلمي ونور دربي

أهدي لهم جميعا هذا العمل

تشكر وعرفان

الحمد لله رب العالمين، على ما أنعم عليّ من نعم وآلاء عظيمة ، والصلاة والسلام على أشرف الأنبياء والمرسلين نبينا محمد وعلى آله وصحبه أجمعين.

يشرفني أن أتقدم بالشكر الجزيل لمشرفي الأستاذ الدكتور: السايح الهباشي على ما أسدى لي من توجيه وإرشاد .

وما يسعدني اكثر أن أنوه بشكري لأساتذتي الذين ما بخلوا عليّ من علمهم بشيء في دراستي والذين سأظل دائماً مديناً لهم وما قدموه . وأتقدم بجزيل الشكر والامتنان لإدارة الكلية و لعميدها الذي الان لنا الصعاب لإنهاء دراستنا على اكمل وجه .

كما يسعدني ان اعبّر عن شكري وامتناني للإخوة بإدارة الشركة العامة للبريد والاتصالات السلكية واللاسلكية ما قدموه لي من عون ودعم وتشجيع لإنهاء دراستي . وتحياتي الى كل من مد لي يد العون لإتمام دراستي.

فجزاهم الله عني خيراً .

Table of Contents

Abstract I
Dedication III
Acknowledgments IV

CHAPTER 1 : Introduction 1

1-1 Introduction 2
1-2 Geography of Libya 3
1-3 Aim of the Thesis 5
1-4 Layout of the Thesis 5

CHAPTER 2 : Previous Studies on the Effect of Sand and Dust Storms on Microwave Links 7

2-1 Introduction 8
2-2 Propagation in Dust and Sand 8
2-3 Previous Work in Countries With Similar Climate 9
2-3-1 Sudan 9
2-3-2 Saudi Arabia 14
2-3-3 Iraq 15

CHAPTER 3 : Radio Wave Propagation 16

3-1 Introduction 17
3-2 Typical Radio Configurations 18
3-2-1 Transmitter 18
3-2-2 Receiver 18
3-2-3 Repeaters 19
3-3 Modulation in Microwave Links 21
3-4 Free-Space Propagation 23
3-5 Path Loss Measurements 27
3-6 Multi-Path Fading 28
3-7 Radio Interference 30
3-8 Other Sources of Reflections 35
3-9 Diversity Measurements 36
3-9-1 Space Diversity 37
3-9-2 Frequency Diversity 39
3-9-3 Cross-Polarized Channels 39
3-10 Rain Attenuation 40

CHAPTER 4 : Samples Collection and Meteorological Data.....42

4-1 Introduction..... 43
4-2 The Data of Dust and Sand Storms.....44
4-3 The Microwave Link from Agedabia to Jalo.....47
4-4 Samples of Dust and Sand.....47
4-5 Analysis of the Samples 48
4-5-1 Libyan Iron and Steel Company Analysis.....49
I- Chemical Composition.....49
II- Particle- Size Distribution (PSD).....51
III- Density and Conductivity.....51
4-5-2 Libyan Petroleum Institute Analysis 52
I- Chemical Composition and Conductivity.....52
II- Particle- Size Distribution (PSD).....53

CHAPTER 5 : Analysis of the Samples.....58

5-1 Introduction.....59
5-2 Calculation of the Dielectric Constant for the Component.....59
5-3 Calculation of the Probability from PSD Analysis.....65
5-4 Estimating the Visibility from Meteorological Data.....68
5-5 Estimating the Wave Attenuation.....71
5-5-1 Method (1).....71
5-5-2 Method (2).....73

CHAPTER 6 : Conclusions and Recommendations 73

6-1 Conclusions 76
6-2 Recommendations 77

References.....78

Appendix (A).....79

Appendix (B).....97
Program (1).....98
Program (2).....100
Program (3).....101
Program (4).....103
Program (5).....105
Program (6).....108

List of Figures

CHAPTER 1

Figure 1.1 Map of Libya....4

CHAPTER 2

Figure 2.1 Map of the Sudan Showing Positions of Abu-Hamad, Atbara, Khartoum and El Obied Cities....10
Figure 2.2 Conditional Probability against Visibility 11
Figure 2.3 Peak Attenuation Values as a Function of Frequency....13

CHAPTER 3

Figure 3.1 Typical Microwave Link....17
Figure 3.2 Types of Microwave Transmitters 19
Figure 3.3 Three Receiver Types Mostly Used 20
Figure 3.4 Types of Digital Radio Repeaters....22
Figure 3.5 Free Space Basic Transmission Loss Versus Path Length..25
Figure 3.6 Fresnel Zones Geometry 27
Figure 3.7 Typical Ground Reflection Parameters....34
Figure 3.8 Fade Depth vs Time Faded for Different Cases....38
Figure 3.9 Specific Attenuation Due to Rain 41

CHAPTER 4

Figure 4.1 Standard Wind Directions Reference....43
Figure 4.2 Map Showing the Sites from Which Data is Collected 45
Figure 4.3 Graph Between the Weight and Radii of Sample 2....53
Figure 4.4 Graph Between the Weight and Radii of Sample 9....54
Figure 4.5 Graph Between the Weight and Radii of Sample 8....55
Figure 4.6 Graph Between the Weight and Radii of Sample 6....56
Figure 4.7 Graph Between the Weight and Radii of Sample 5....57

CHAPTER 5

Figure 5.1a PSD Curves from Libyan Iron and Steel....67
Figure 5.1b PSD Curves from Libyan Petroleum Institute 67
Figure 5.2 The Relation Between Attenuation and Visibility 72
Figure 5.3 The Relation Between Attenuation and Visibility 74

List of Tables

CHAPTER 2

Table 2-1 The Average Number of Hours of Visibility in Four Towns.....10

Table 2-2 The Attenuation in dB/km for the Two Types of Dust.....13

CHAPTER 4

Table 4-1 Wind Speed for Agedabia 46

Table 4-2 Wind Speed for Jalo 46

Table 4-3 Place and Type of Samples 48

Table 4-4 Libyan Iron and Steel Analysis/ sample (1) 50

Table 4-5 Libyan Iron and Steel Analysis/ sample (2) 50

Table 4-6 Libyan Iron and Steel Analysis / four samples 50

Table 4-7 Libyan Iron and Steel Analysis/ sample (2) 51

Table 4-8 Libyan Iron and Steel Analysis/ sample (3) 51

Table 4-9 LISCO Analysis for Density and Conductivity.....51

Table 4-10 Libyan Petroleum Institute for Five Samples.....52

Table 4-11 PSD of sample (2).....53

Table 4-12 PSD of sample (9).....54

Table 4-13 PSD of sample (8).....55

Table 4-14 PSD of sample (6).....56

Table 4-15 PSD of sample (5).....57

CHAPTER 5

Table 5-1a From LISCO Analysis of Sample (1) 59

Table 5-1b Results of sample (1) after Normalization 60

Table 5-2a From LISCO Analysis of Sample (2) 60

Table 5-2b Results of sample (2) after Normalization 61

Table 5-3a From LISCO Analysis of Sample (3) 61

Table 5-3b Results of sample (3) after Normalization 62

Table 5-4 From LISCO Analysis of Sample (4) 62

Table 5-5a From LISCO Analysis of Sample (5) 62

Table 5-5b Results of sample (5) after Normalization 63

Table 5-6 From LISCO Analysis of Sample (6) 63

Table 5-7 From LISCO Analysis of Sample (10) 63

Table 5-8 Results from LISCO 64

Table 5-9 Results When the Sample is Normalized 64

Table 5-10a PSD for S. (2) from the Libyan Petroleum Institute.....65

Table 5-10b PSD for S. (9) from the Libyan Petroleum Institute.....66
Table 5-10c PSD for S. (8) from the Libyan Petroleum Institute.....66
Table 5-10d PSD for S. (6) from the Libyan Petroleum Institute.....66
Table 5-10e PSD for S. (5) from the Libyan Petroleum Institute.....66
Table 5-11a The Visibility in Agedabia 69
Table 5-11b The Visibility in Jalo 69
Table 5-12 Average of Visibility in Jalo and Agedabia 70
Table 5-13 The Value of Attenuation (Method 1) 72
Table 5-14 The Value of Attenuation (Method 2) 74

CHAPTER 1

Introduction

1-1 Introduction

The millimeter wave band provides the potential for more services than all of the lower radio bands together, unfortunately, the shorter the wavelength the more attenuation will be induced by absorption and scattering due to rain, dust and sand particles in the radio path. If the excess attenuation exceeds the available fade margin, the result is service interruption and system outage. For frequencies below 10 GHz, the common practice has been that the allowed outage time is allocated to equipment failure and fading. Excess attenuation due to hydrometers and other particles can be significant below 10 GHz, particularly in tropical areas. In the millimeter wave band, however, the practice was revised to allow more margins for rain and other effects induced attenuation. to meet reliability objectives, shorter hops must be used for moderate rain areas and wet regions, with shorter hops, most of the outage budget can be allocated to rain attenuation since significant refractive fading is less likely to occur on a short hop. In dry areas, marked by less than 200 mm of total rainfall per year, (as is the case for some parts of Libya) longer hops can be operated in the millimeter wave band with acceptable reliability. however, such areas are subject to frequent sand and dust storms during which particles of sand and dust may rise high enough above the ground to obstruct the radio beam either by attenuating or by cross polarizating it, Such storms may last for minutes or days, reducing visibility to several kilometers or as little as a few meters.

"In the literature the particles with radii less than 60 micron termed clay or silt, and the dust used to refer to airborne particles with radii less than 60 micron. Airborne particles with radii greater than 60 micron maintain the name sand, these are the definitions used by [1]". Dust storms are frequently mislabeled as "sandstorms." these are two different

phenomena, dust storms usually occur over arable land where there has been a drought over extended periods, strong winds may raise the fine surface particles, referred to as dust, as high as one kilometer. The particle diameters are generally less than 80 μm and may be as small as 10μm. Hence, the fall speeds of such particles are such that the dust may obscure the sun for extended periods. To be classified as a dust storm, the visibility must be smaller than 1 km. When the visibility is shorter than 500 m, it is called a "severe dust storm" [1] .

Libya with total area around 1.75 million square kilometers most of it is desert, in a most situation for microwave links at some parts that has too high dust and sand storms, this necessitate the finding of the chemical composition of the dust and sand, then estimation of the attenuation due to these storms. There is no such a study before this that is linked directly to Libya soil properties so this work will be the first to do so.

1 -2 Geography of Libya

Location: Northern Africa, bordering the Mediterranean Sea, between Egypt and Tunisia

Geographic coordinates: 25 00 N, 17 00 E

Map references: Africa Area: total: 1,759,540 sq km

border countries: Algeria 982 km, Chad 1,055 km, Egypt 1,150 km, Niger 354 km, Sudan 383 km, Tunisia 459 km as show in Fig.(1.1)

Coastline: 1,770 km . Maritime claims: territorial sea: 12 NM .

Note: Gulf of Sirte closing line - 32 degrees, 30 minutes north

Climate: Mediterranean along coast; dry, extreme desert interior

Terrain: mostly barren, flat to undulating plains, plateaus, depressions

Elevation extremes: lowest point: Sabkhat Ghuzayyil -47 m

Natural resources: petroleum, natural gas, gypsum

Land use: arable land: 1%. Permanent pastures: 8% .

Forests and woodland: 8%

Natural hazards: hot, dry, dust-laden glibly is a southern wind lasting one to four days in spring and fall; dust storms, sandstorms

Environment - current issues: desertification; very limited natural fresh water resources; the Great Manmade River Project, the largest water development scheme in the world, is being built to bring water from large aquifers under the Sahara to coastal cities .

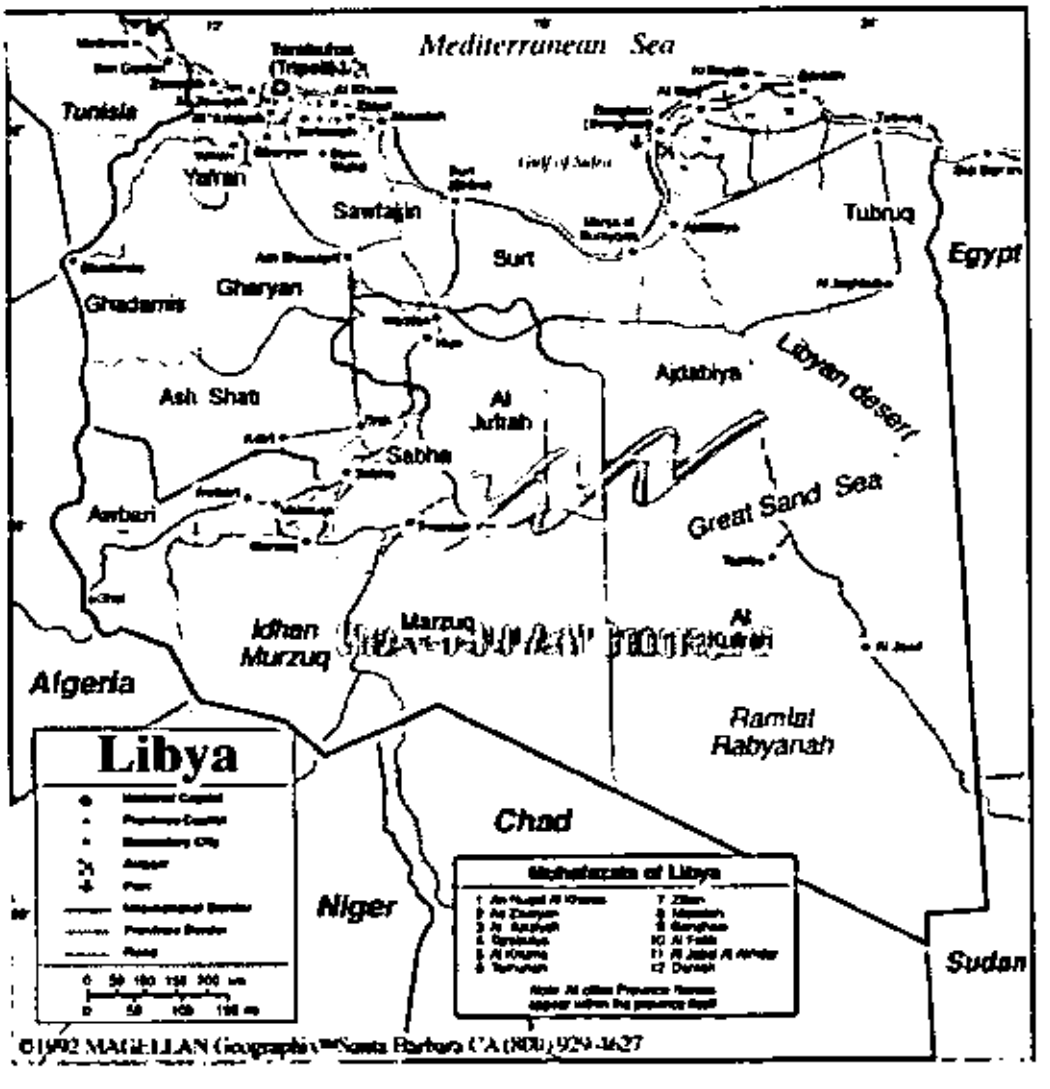

Fig. (1.1) Map of Libya

1-3 Aim of the Thesis:

The main aim of this thesis is summarized in the flowing points:-

- Reviewing the effect of sand and dust storms on microwave link.
- Getting the chemical composition of dust and, sand as well as the equivalent dielectric constant.
- Collecting the meteorological data for two cities in for region of this study for last ten years (Agedabia, Jalo) .
- Studying the effect of sand and dust storms on microwave link from Agedabia to Jalo cities.
- Computing the attenuation effect of sand and dust storms on LOS at the area of case study.

1-4 Layout of the Thesis:

This thesis consists of five chapters in addition to the introductory chapter as follows

- Chapter 2 "**Previous Study on the Effect of Sand and Dust Storms on Microwave Links**", This chapter describes and looks at literature review on the previous studies done on the effect of sand and dust storms on microwave links in neighboring countries
- Chapter 3 "**Radio Wave Propagation**" This chapter explains the general introduction, typical radio system, modulation in microwave links, free space propagation, path loss measurements, multi-path fading and diversity measurements.
- Chapter 4 "**Samples Collection and Meteorological Data**" This chapter includes the general introduction, dust and sand data, with their lab analysis and results, as well as wind speed data.

- Chapter 5 " **Analysis of the Results"** This chapter contains the analysis of the data presented in chapter 4 and mainly it founds the dielectric constant, the probability distribution density and estimate the visibility from the will find the attenuation to the microwave signal of the microwave link.

- Chapter 6 **"Conclusion and Recommendations"** This chapter include the main conclusions of this work and suggest some points as a future work.

CHAPTER 2

Previous Studies on the Effect of Sand and Dust Storms on Microwave Links

2-1 Introduction:

This chapter gives the essential bake ground needed for the subject of this thesis, and looks at previous work done in countries with similar climate conditions to that in Libya.

2-2 Propagation in Dust and Sand:

The propagation of microwave signals in a dusty media (air with suspended soil particles) find a considerable interest recently; due to

(i) The large development in radio links established in areas where dust and/or sand storms are frequently encountered.

(ii) The introduced frequency reuse technique in some of these links. When the operating frequency above 1 GHz echoes from various particles such as dust, may become significant.

In order to predict the dust dielectric constant from it's minerals and/or chemical composition values, the following points should be considered:

1) Chemical and mineral composition of the dust

2) The dielectric constant of each constituent

3) A model for the mixture dielectric constant.

The earth surface is composed of a large number of minerals nonhomogeneous mixture form, which means that dust and sand is expected to have similar composition as that of the parental soil, but it's percentage may vary.

Several investigators studied the effect of sand and dust on a microwave signal [2].

The attenuation coefficient due [α] to dust may be expressed by

the formula or the formulation given in [2].

$$\alpha = W\left(\frac{1}{\lambda}\right)\left(\frac{1}{V^{1.07}}\right) \quad [dB/km]$$

Where :

λ is the wavelength in meters,

V is the visibility in kilometers،

W is a constant based on the dielectric constants measured in X band, $W=1.94\times10^{-5}$ (for 4% water), $W=1.60\times10^{-5}$ (for 2% water), and $W=1.15\times10^{-5}$ (for 0% water).

"The expression applies to frequencies at or in the vicinity of X band since the calculation is based on dielectric constants measured in this band ". [2].

2-3 Previous work in countries with similar climate:

The effects of sand storms on the propagation have been considered by only few investigators in Sudan , Iraq and Saudi Arabia this is because most of the developed countries do not face this problem,

and they have completely different problem due to rain and snow

2-3-1 Sudan:

In one of his work was carried out by S. I. Ghobrial [1] where he selected four towns in Sudan as shown on the map in Fig. (2.1) .

The measured visibility at these towns is listed in Table(2-1) . He gave the statistics of visibility as observed in the four towns. These are the average of observations made over five years period. The number of hours is the total time of visibility within the range indicated.

Fig.(2.2) represents the average yearly conditional cumulative distribution of visibility averaged over a five-year period and combined over four sites locationed in Sudan

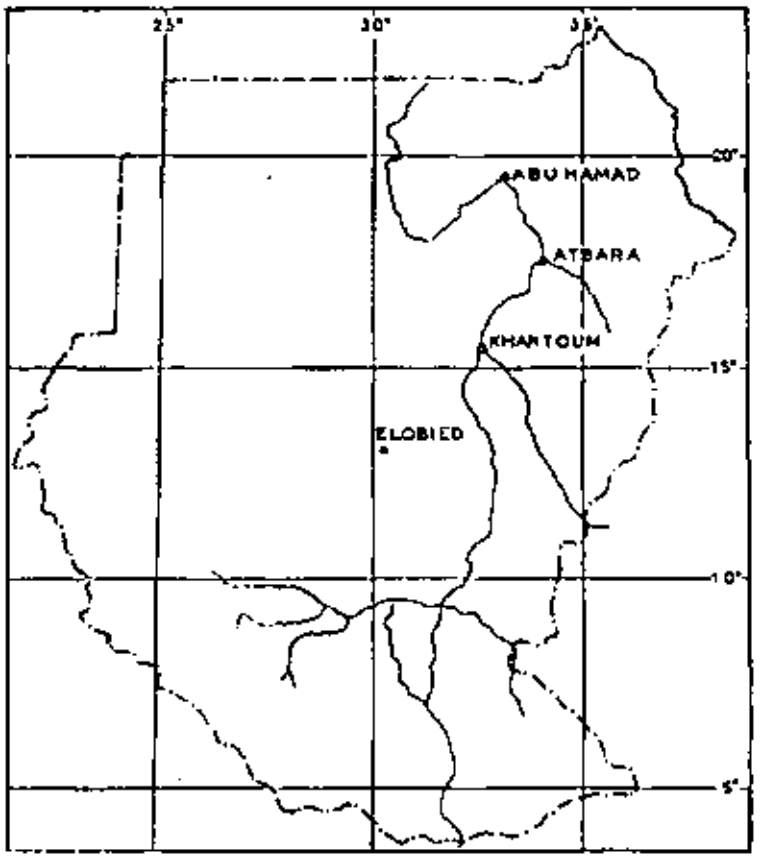

Fig. (2.1) Map of the Sudan Showing Positions of Abu-Hamad, Atbara, Khartoum and El Obied

Table(2-1)The Average Number of Hours of Visibility in Four Towns

Visibility (meter)	0-100	100-200	200-300	300-400	400-500	500-600	600-700	700-800	800-900	900-1000
Town	Hrs/annum									
Khartoum	3.80	5.40	6.13	7.27	6.75	8.41	3.77	2.63	21.64	0.79
Abu-Hamad	0.61	4.52	4.03	7.53	2.45	15.16	19.62	6.83	17.34	9.11
El Obied	2.37	4.03	6.22	3.77	4.20	4.56	2.63	0.35	13.67	1.40
Atbara	0.79	1.59	1.60	6.18	3.85	6.75	8.76	10.16	17.43	4.38

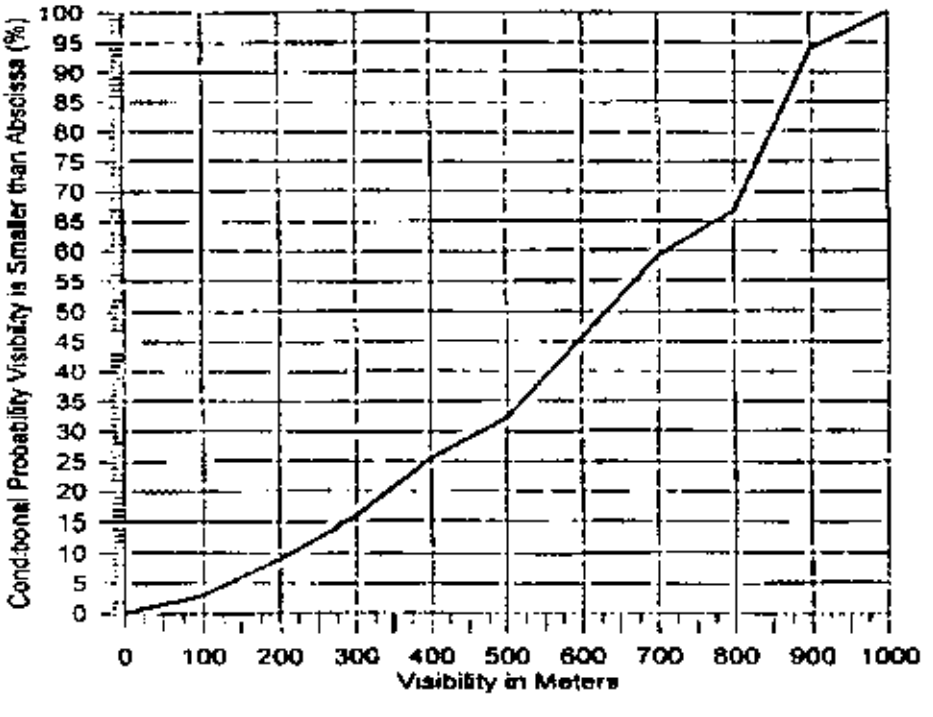

Fig. (2.2) Conditional Probability against Visibility

The results of Fig. (2.2) show the occurrence of a dust storm with a visibility smaller than 50 m is approximately 1.3 h on the average during the year. And the average measured density (ρ) of nine samples collected in Khartoum, is given by $\rho = 2.44 \times 10^3$ kg/m^3.

For visibilities greater than 0.1 km attenuation is less than 0.2 dB for a path length of 20 km. In general for visibilities better than 200 m attenuation is negligible for both linear and circular polarization. For visibilities less than 200 m attenuation increases rapidly with decreasing visibility. This is primarily due to the increase in phase difference between horizontal and vertical polarizations. For visibility of about 5.5m the phase difference becomes 9°/ km. For a path of 20 km the angle φ becomes 180° and attenuation reaches a maximum. [1].

The chemical compositions of typical samples collected in Khartoum are by weight 62% silicon dioxide, and 38% other metallic oxides including iron and aluminum. The diameters of most sandstorm particles are greater than 0.08 mm and are usually between 0.15 and 0.3 mm. Sand particles are usually comprised of 92% silicon dioxide by weight. "The moisture concentration of the soil is 5% at 14, 24, and 37 GHz, where as the soil moisture concentration of the soil is 2% at 3 and 10.5GHz" [2].

The dielectric constant of dust collected from central Sudan and sand collected from northern Sudan were found to be different because of their different chemical compositions and not because of the difference in grain or particle sizes because of that the attenuation experienced by a linearly polarized wave in dust storms is negligible except for the case of very severe storms with visibilities of a meter or less. Table (2-2) gives attenuation in dB/km for the two types of dust considered above for the different visibilities. The effects of storms on microwave propagation were investigated; it was found that for linear polarization the effect of dust storms is almost negligible except for very dense storms. For circular polarization, cross polarization can be serious when visibilities fall below 100 m over about 10 km of path, or below 10 m over about 1 km of path. this would require extremely severe dust conditions at frequencies around 10 GHz.[1],there finding does not agree with the results presented by J. Goldirsh [2] on the same data were he reported path attenuation of 2.5dB at 5 GHz to 15dB at 20 GHz as shown in Fig.(2.3) . The peak path attenuation would reach a level of 22.6 dB at 37 GHz.

Table (2-2) The Attenuation in dB/km for the Two Types of Dust

Visibility (km)	$\epsilon = 5.23 - j0.26$			$\epsilon = 6.23 - j0.57$		
	α_v(dB/km)	α_h(dB/km)	m	α_v(dB/km)	α_h(dB/km)	m
1.000	2.57×10^{-4}	4.90×10^{-4}	0.99997	4.10×10^{-4}	8.57×10^{-4}	0.99995
0.500	5.27×10^{-4}	1.03×10^{-3}	0.99994	8.61×10^{-4}	1.80×10^{-3}	0.99989
0.100	2.95×10^{-3}	5.76×10^{-3}	0.99968	4.82×10^{-3}	1.01×10^{-2}	0.99940
0.050	6.19×10^{-3}	1.21×10^{-2}	0.99932	1.01×10^{-2}	2.11×10^{-1}	0.99873
0.010	3.46×10^{-2}	6.76×10^{-2}	0.99621	5.66×10^{-2}	1.18×10^{-1}	0.99292
0.005	7.27×10^{-2}	1.42×10^{-1}	0.99206	1.19×10^{-1}	2.48×10^{-1}	0.98520

The backscatter properties of sand storms had been investigated by Sharief and others in a couple of publications, full theory and resulted has been reported [2].

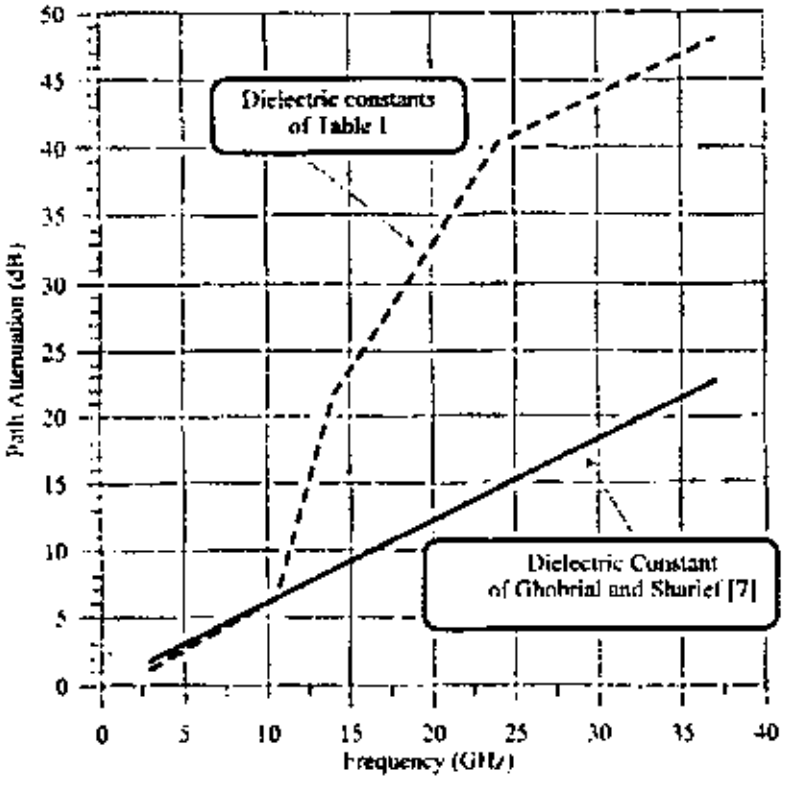

Fig. (2.3) Peak Attenuation Values as a Function of Frequency

2-3-2 Saudi Arabia

A. Ali [3] presented a procedure for obtaining the optimum hop length for millimeter wave radio links operating in arid and semi-arid regions, the procedure is based on long-term meteorological data for Saudi Arabia, a typical arid land, and a set of actual field measurements from a millimeter-wave radio network, his results were based on a study of the meteorological data obtained include a 25-year rain and sandstorm record from 137 recording stations in Saudi Arabia. The study involved the operation and monitoring of radio links in the millimeter wave and infrared parts of the spectrum. Meteorological stations and related test equipment were also operated and monitored. The experimental system comprised:

(I) A set of three radio links: two millimeter waves (40 GHz) and one near infrared (0.88 m) with path distances of 14 km and 0.75 m.

(ii) Meteorological instrumentation including dust passive collectors, high volume samplers and a dust particle-size analyzer.

" Predicting attenuation and phase shift caused by sand or dust storms requires knowledge of pertinent storm parameters affecting propagation. Such parameters include particle shape, size distribution, refractive index, concentration and composition. A record of all sand and dust storm events which occurred in Saudi Arabia over 20 years from 1968 was obtained from the Meteorological & Environmental Protection Administration (MEPA). It includes the dates and durations when the optical visibility was reduced due to storm events. An analysis of propagation reliability for millimeter wave radio links operating in an arid climate has been presented. Using the results of actual measurements of excess attenuation due to rain, sandstorms and fading at 40 GHz in Riyadh. The results are presented in the form of design charts depicting

link reliability against fade margin at various hop lengths. The frequency band from 30 to 70 GHz was covered in 10 GHz increments. Sand particle sizes of 0.07 and 0.15 mm were considered with moisture contents of 0%, 5% and 10%. Different design charts were given for various geographical regions of Saudi Arabia. It is believed that the analysis will be used by radio engineers designing radio links operating at Millimeter wavelengths in an arid climate". [3].

2-3-3 Iraq

Shakir and H.M. Al-Rizzo [4] In their work several windblown and dust fall samples were collected in the spring, summer and autumn of 1984 at a height of 20 m above the ground surface during severe sand and dust storms over the city of Baghdad, Iraq. The particle-size distribution (PSD) of the samples was determined using five different measurement techniques (hydrometer, pipette, sedimentation balance, optical microscope and coulter counter). The results showed that the cumulative weight techniques yield almost identical results for all the samples tested. The mode of the number distribution was found to occur at around 2 and 3.5 μm for the blowing and falling dust samples, respectively. A computer program was developed to describe the measured distributions by some analytical functions. It was found that the cumulative distributions can be well described by a third degree polynomial and log-normal functions for particle diameters ranging from 1 to 100 μm. An attempt has been made to estimate the attenuation α and phase shift β for a microwave signal for up to 37 GHz utilizing the measured PSD and for different particle moisture contents. It was concluded that at 37 GHz and for 10 m visibility, the upper bound for α and β were 0.7 dB/km and 26.5 degree/km for 20 percent particle moisture content

CHAPTER 3

Radio Wave Propagation

3-1 INTRODUCTION :

A microwave link is the name given to a point-to-point link using the propagation of electromagnetic waves at microwave frequencies through free space as shown in Figure (3.1). [6] .

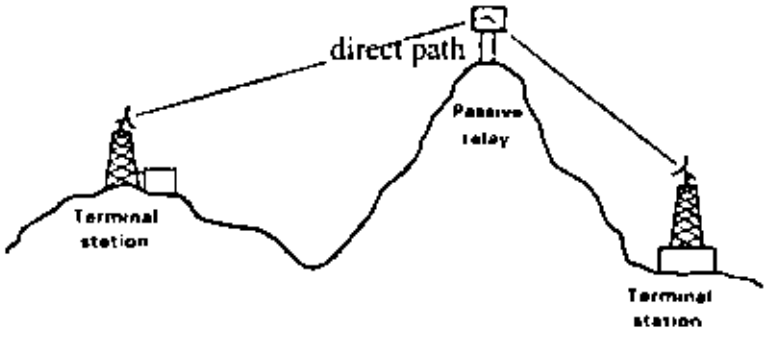

Fig. (3.1) Typical Microwave link

The radio frequencies above 30 MHz, has the tendency to penetrate the ionosphere making them unsuitable for long distance propagation. The range of frequencies from 30 to 300 MHz, are mainly used for line-of-sight communication. Under many propagation conditions, the loss or gain of signal due to the atmosphere is uniform across the radio channel bandwidth; an example is the loss due to extreme rainfall rate or very strong dust storm. The digital links are typically more resistant to these types of fades it also gives the following advantages over analogue links.

- It removes distortion arising during transmission and gives a better link quality than that obtained with analogue transmission.
- For signal processing, it is well suited to all types of data and information to be transmitted and it uses components designed for computers, which contributes towards a reduction in the cost of equipment.

When the signal loss imposed by the atmosphere varies across the frequency band occupied by a radio channel, the channel is said to be experiencing selective fading other wise it is called flat fading.

3-2 Typical Radio System :

Every radio system consists, in it's simplest of a transmitter, a receiver and in some cases a repeater.

3-2-1 Transmitter:

The two basic transmitter categories for digital microwave transmission are the directly modulated type, which modulates the radio-frequency carrier with the base band signal (usually without subsequent amplification), and the indirect heterodyne type, which accepts a modulated IF signal as input, translates it to RF, and amplifies it to a power level appropriate for transmission, examples of these are shown in Figure (3.2).Transmitters of the direct modulation type usually either amplitude shift key (ASK) or frequency shift key (FSK) the RF microwave oscillator, or phase shift key (PSK) the output of a microwave oscillator with a modulator external to the RF source. The path length modulator has been used as a PSK modulator. It introduces an additional path length (using diode switches) to achieve a phase shift (e.g., $\lambda/2$ for 180°,$\lambda/4$ for 90°, et cetera).

Virtually all modulations may be indirectly generated at IF and used with the heterodyne-type transmitter, but the most widespread IF modulator applications are in linear transmitters for high capacity digital radio [5].

3-2-2 Receiver:

Most microwave digital radio receivers are of the single-conversion heterodyne type. In receivers which must be of the frequency

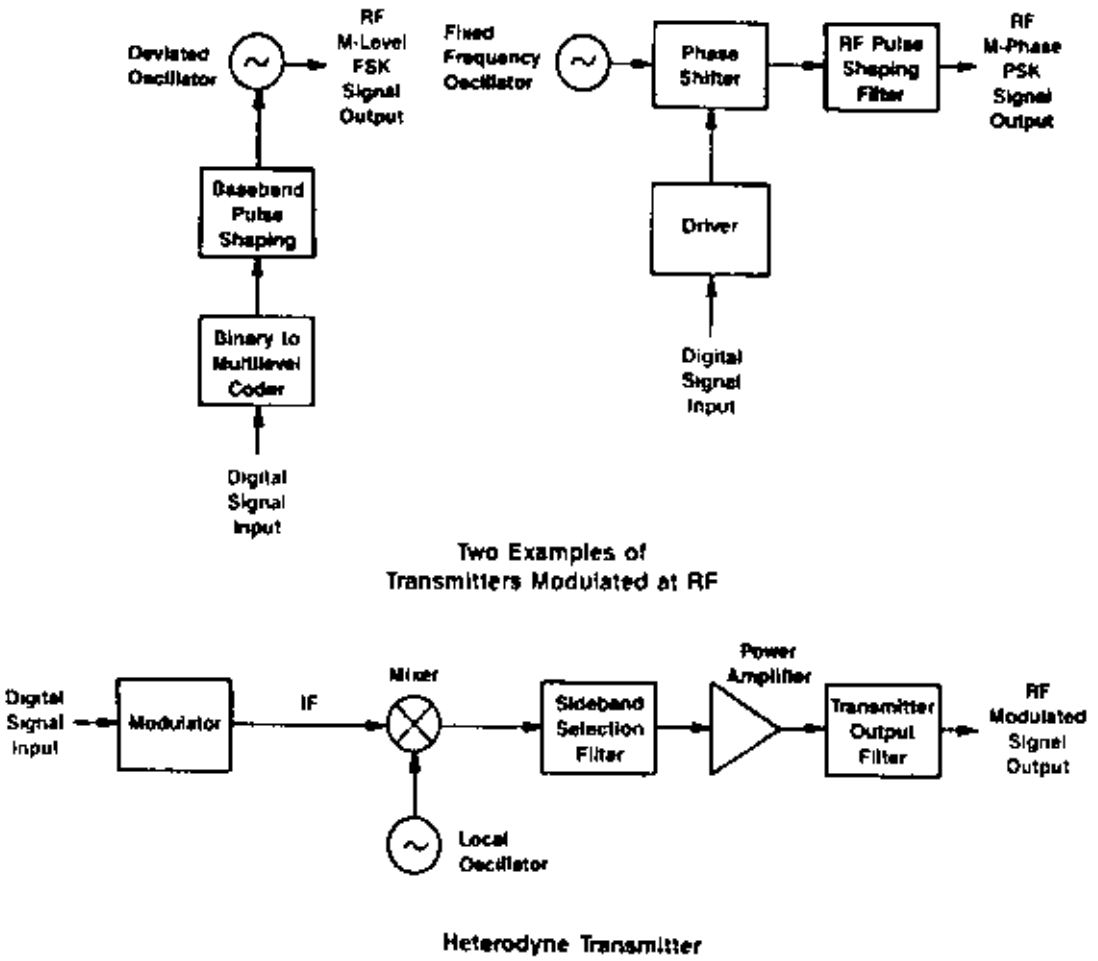

Fig. (3.2) Types of Microwave Transmitters

agile, it may be advantageous to have a second intermediate frequency. Direct demodulation at RF is feasible, but it has only been used commercially in a few instances. Block diagrams of three receiver alternatives are shown in Figure (3.3).

3-2-3 Repeaters:

A microwave digital radio repeater consists of the equipment to receive an RF- modulated signal at one frequency, amplify it, and usually shift it according to an RF channelization plan to another frequency for retransmission, in the process, the signal may be shifted to a much lower intermediate frequency where amplification, space-diversity combining,

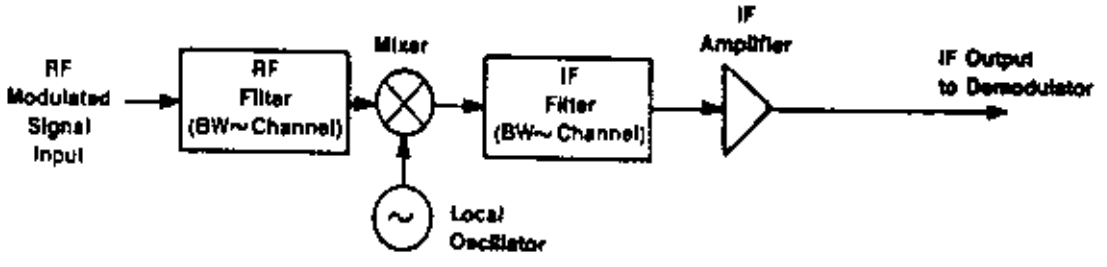

Single Conversion Heterodyne

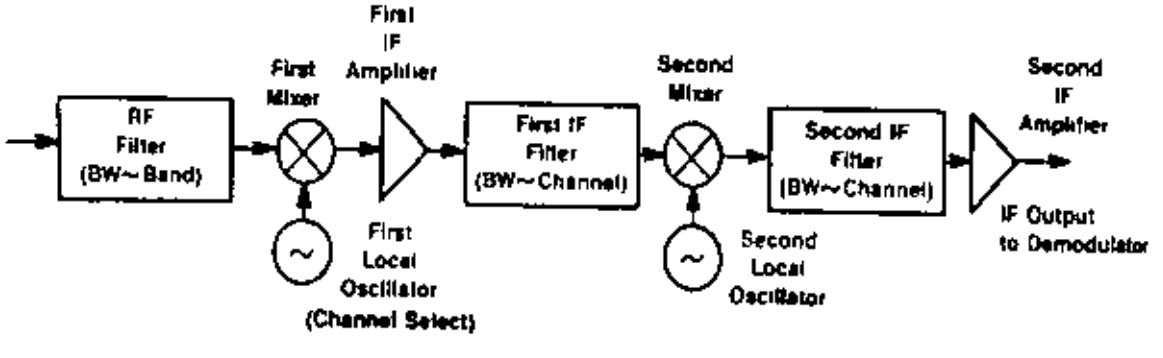

Double Conversion Heterodyne

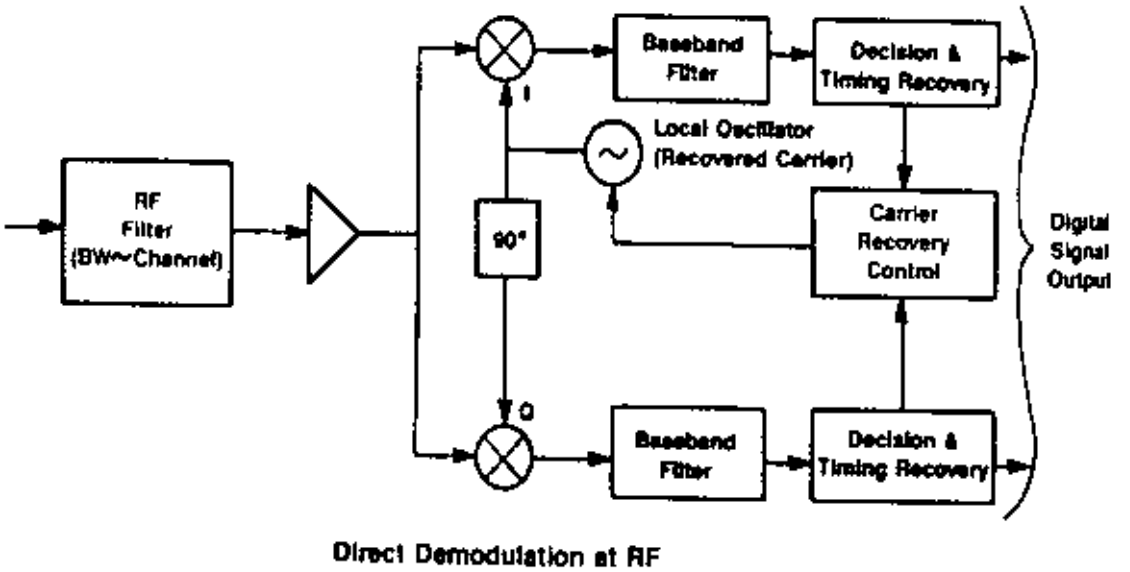

Direct Demodulation at RF

Fig. (3.3) Three Mostly Used Receiver Types

and frequency-domain equalization can be performed economically. It may then be demodulated, regenerated, and remodulated either at RF or at IF, with subsequent shifting to the repeater output frequency. As shown in the block diagram in Figure (3.4), the main parts of a repeater are:

- A heterodyne receiver and heterodyne transmitter with IF interfaces to the demodulator and modulator, respectively.
- A heterodyne receiver with an IF interface to the demodulator-regenerator equipment, which in turn interfaces with a directly modulated transmitter at base band.
- A nonregenerative heterodyne repeater (i.e., a heterodyne receiver and a heterodyne transmitter interconnected at IF with no intervening demodulator-regenerator-modulator equipment).
- An RF nonregenerative repeater without frequency shifting.

The first type is most commonly used in medium and high capacity systems. The second is often used in small capacity systems, and in systems operating at higher microwave frequencies. The third type is still undergoing many developments, one system allows the shared use of the protection channel with an analog radio system on the same route, and lessens the amount of equipment required. The fourth type, the nonregenerative direct RF repeater is essentially a band limited RF amplifier for each direction of transmission, which has been used in a number of different applications [5].

3-3 Modulation in microwave links:

The carrier wave in a microwave link suffers a fluctuating attenuation of its amplitude during propagation, in addition, some of the elements in the microwave circuits have a non-linear amplitude response, the amplitude distortion of the carrier wave produced by these effects means that amplitude modulation is unsuitable for such links, angle modulation, on the other hand, is almost unaffected by the propagation conditions or by the non-linear amplitude response of equipment, it also

Heterodyne Receiver and Transmitter with IF Regenerator

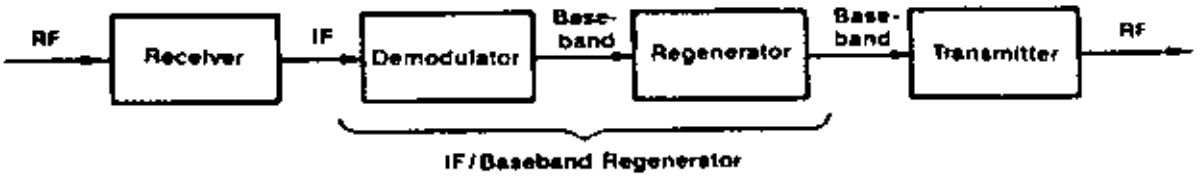

Heterodyne Receiver, IF/Baseband Regenerator and Directly Modulated Transmitter

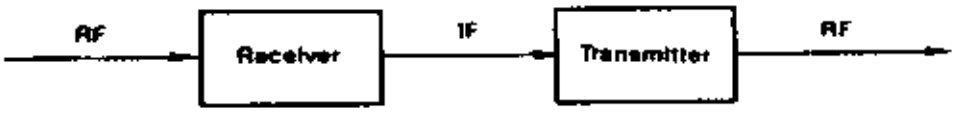

Non-regenerative Heterodyne Repeater

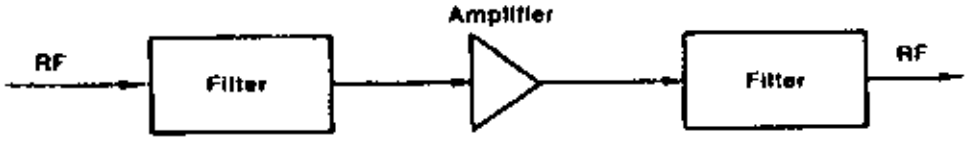

All RF Non-regenerative, Non-frequency Shifting Repeater

Fig. (3.4) Types of Digital Radio Repeaters

provides good protection against noise and most electronic interference, which affects only the carrier amplitude, as a result, by far the largest number of analogue microwave links use angle modulation for:

1-Transmission of analogue telephone multiplexes with capacities up to 2700 channels.

2- Medium- and high-speed telex or data transmission.

3- Transmission of television video signals.

Digitally modulated microwave links, under normal propagation conditions, produce an almost perfect quality since, the signal can be more easily regenerated than with analogue modulation for the same signal-to-noise ratio, if the propagation conditions deteriorate, however, signal regeneration is no longer possible with digital modulation as soon as the signal-to-noise ratio falls below a certain threshold value, where as it is still possible with analogue modulation.

Digitally modulated microwave links are used for :

1- The transmission of digital telephone multiplexes with speeds of up to 140 Mbit/s

2- High-speed transmission of digital data

3- Video phones and encoded television.

2-4 Free-Space Propagation:

The propagation of signals on LOS microwave radio paths is affected by both the atmosphere and the intervening terrain. The reference for describing propagation effects is the free-space basic transmission loss, this is the loss that would occur if the antennas were replaced by isotropic antennas located in a perfect dielectric, homogeneous, isotropic and unlimited environment, with the distance between the antennas being retained. The loss between terminals of such hypothetical antennas is called the free space basic transmission loss, L_{bf} and is expressed in decibels [5].

$$L_{bf} = 92.45 + 20 \log f_{GHz} + 20 \log d_{km} \quad \text{dB} \quad \ldots\ldots\ldots\ldots (3-1)$$

The frequency f is in gigahertz, d is the path distance in kilometers.

The solution to this equation is presented graphically in Figure (3.5) for

various frequencies and distance ranges.

In free space, the energy is assumed to propagate from the transmitting antenna to the receiving antenna along a single ray path labeled the direct path in Figure (3.1). The effects of terrain features on propagation conditions are usually related to the geometric position of these features with respect to the Fresnel zones of the path, an understanding of them is basic to considerations of path clearances, for instance, since about half of the signal energy reaching the receiving antenna passes through the first Fresnel zone, terrain features that do not intrude into this zone cannot significantly alter the level of the received signal. The first Fresnel zone is the region of space that contains all of the two-segment paths that have a composite length exceeding that of the direct path by less than half a wavelength, $\lambda/2$, clearly, the boundary of the first Fresnel zone is an ellipsoid, higher order Fresnel zones are defined in a similar manner. thus, the second zone contains all those points that define two-segment paths for which the length is greater than the direct path by more than $\lambda/2$, but less than $2(\lambda/2)$. Hence the Fresnel zones form a nested set of ellipsoidal shells [5].

The Huygens-Fresnel wave theory states that the electromagnetic field at a point, S_2 , Figure (3.6) is due to the summation of the fields caused by re-radiation from small incremental areas over a closed surface about a point source, S_1, provided S_1 is the only primary source of radiation, The field at a constant distance, r_1, from S_1 (a spherical surface) has the same phase over the entire surface since the electromagnetic wave travels at a constant speed in all directions in free space. This constant phase surface is called a wave front. If the distances, r_2 , from various points on the wave front to S_2 are considered, the contributions to the field at S_2 will be seen to be made up of components that add vectorially

in accordance with their relative phase differences. Where the various values of r_2 differ by $\lambda / 2$ (half wavelength), the strongest cancellation occurs (out of phase addition).Fresnel zones distinguish between the areas on a closed surface about S_1 which add and those which cancel [7].

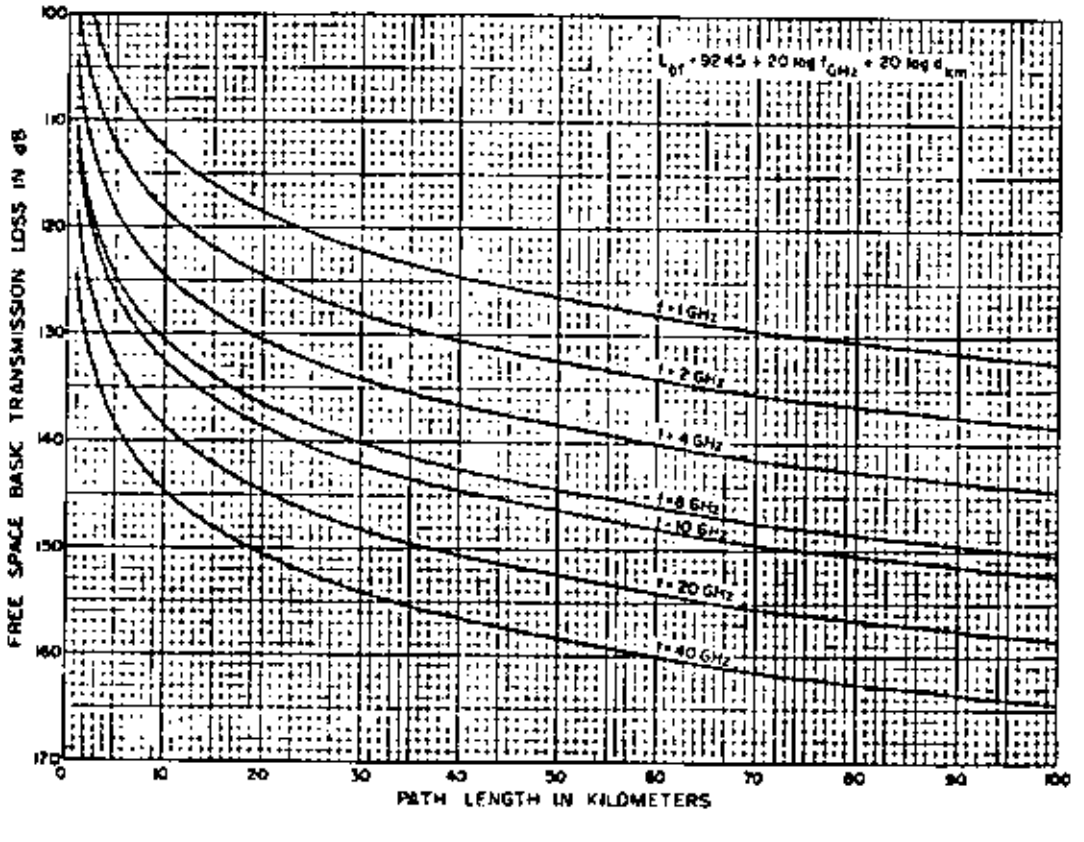

Fig.(3.5) Free Space Basic Transmission Loss Versus Path Length

Consider a moving point, P, in the region about the terminal antenna locations S_1 and S_2 such that the sum of the distances r_1 and r_2 from the antennas to P is constant, such a point will generate an ellipsoid with S_1 and S_2 as its foci. Defining a set of concentric ellipsoidal shells so that the sum of the distances r_1 and r_2 differs by multiples of the half wavelength ($\lambda / 2$). The intersection of these ellipsoids with any surface defines Fresnel zones on the surface, thus, on the surface of the wave front, a "first" Fresnel zone F1 may be defined as bounded by the intersection with the sum of the straight line segments r_1 and r_2 equal to

the distance d plus one-half wavelength ($\lambda / 2$) The second Fresnel zone, F2, is defined by the region where ($r_1 + r_2$)is greater than [$d + \lambda / 2$] and less than [$d + 2 (\lambda / 2)$]. Thus, Fn is the region where ($r_1 + r_2$)is greater than [$d + (n - 1) \lambda / 2$] but less than ($d + n \lambda / 2$) .

Field components from even Fresnel zones tend to cancel those from odd zones since the second, third, and fourth zones, etc., are approximately equal in area.

The concept of Fresnel zones is not meaningful for the "near field" within short distances of practical antennas. A rule of thumb for determining the minimum distance d_F, at which the zones become meaningful is that d_F be greater than ($2D^2/\lambda$), where D is the maximum dimension of the antenna aperture in the same units of length as λ .

A good approximate equation (valid for almost all microwave applications) for the outside boundary of the n^{th} Fresnel zone radius, R_n , on a surface perpendicular to the propagation path is

$$R_n = \left(n\lambda \left(\frac{d_1 d_2}{d_1 + d_2} \right) \right)^{1/2} \qquad \text{..... (3-2a)}$$

or

$$R_n = 17.3 \left(\left[\frac{n}{f_{Ghz}} \right]^{1/2} \left(\frac{d_1 d_2}{d_1 + d_2} \right) \right)^{1/2} \qquad \text{..... (3-2b)}$$

d in Km

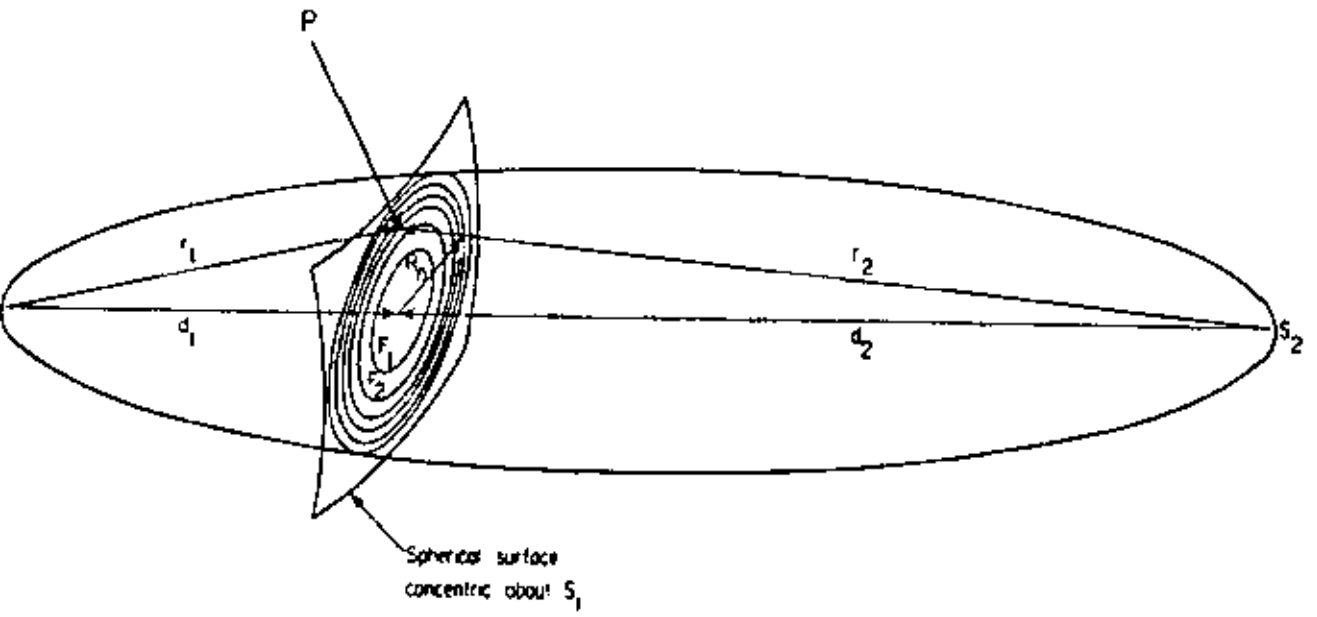

Fig. (3.6) Fresnel Zones Geometry

In the first equation (3-2a) all distances and the wavelength must be in the same units and must be small compared to the distance and antenna heights involved. r_1+r_2 should not be significantly larger than d_1+d_2 . In the second equation all distances are in kilometers, the frequency is in GHz and the Fresnel zone radius is in meters. If R_i is the radius of the i^{th} Fresnel zone, then

$$R_n = R_1(n)^{1/2} \qquad \text{.....} \qquad (3\text{-}3)$$

Because the higher numbered zones tend to be self canceling, they are not significant for many calculations; however, consideration of the higher order zones is helpful in understanding obstacle diffraction, or the use of diffraction gratings as passive repeaters.

3-5 Path Loss Measurements:

Path loss tests, if required, are made by transmitting an un modulated RF carrier between adjacent repeater sites and measuring the received power levels over a period of time and in some cases for various

combinations of antenna elevations. Path loss as a function of time and antenna height is readily determined from such data if transmitter power, antenna gains, and waveguide losses are known.

Path loss measurements are not usually necessary on carefully designed LOS radio links, there are paths, however, where it may be advisable to make such tests prior to facility construction, if, for example, antennas of the heavy horn-reflector type are to be used, the antenna position on the tower cannot easily be changed once the installation is completed, in such cases height-gain measurements may help in determining the optimum antenna position. "Measurements are also recommended on any path where there is a possibility of strong ground reflections, or on paths where design calculations indicate borderline conditions of fading margin or Fresnel-zone clearance. These problems might arise where the choice of suitable sites is limited, or local zoning restricts tower heights (near airports, as an example)"[7].

"Manpower and equipment required for path loss testing make it an expensive operation, temporary towers are usually required at both sites as are some means of moving the antenna quickly from one position on the tower to another, portable power units will also be needed, in addition to . a stable transmitter and receiver, recording equipment, transmission lines, and calibration equipment. The tests must be made over exactly the same path as that intended for the final installation, and in rough or heavily wooded terrain it may be nearly impossible to make measurements until the sites have been acquired, ground cleared, and access roads provided"[7].

3-6 Multi-path Fading:

"Multi-path effects occur in two forms: reflection from the ground or water surfaces, and refraction or reflection by in homogeneities in the

atmosphere. Under some circumstances, the direct ray will be interfered with by the ground-reflected ray or other multi-path rays, the most severe fading occurs when there are two effective components of the same order of magnitude varying in their relative phase. "Measurements made in the United State show that as many as six significant components may exist at one time" [7].

Multi-path propagation measurements carried out in Japan "showed that most of the deep fades are caused by destructive interference between two dominant rays and that the path-length difference between these rays varies to a considerable extent from path to path. Maximum path length differences on the order of many wavelengths can be observed on over sea as well as on overland paths"[7].

Very severe fading can occur on over-water paths when the point of specular reflection falls on the water, if such a path cannot be avoided, space or frequency diversity may be used to reduce the severity of the fading, alternatively, fading can be reduced considerably if the geometrical point of reflection on the water is screened from one or the other of the terminals by the terrain, even if some of the surface of the water is still visible from both terminals.

Under normal conditions and over moderately rough sea or irregular terrain, one expects a portion of the ground-reflected wave to be scattered out of the propagation path, however, when the atmosphere is super-refractive and the surface appears concave, the reflected wave is enhanced by the convergence of the associated rays. The frequency of occurrence and observation of multi-path fading caused by layering in the atmosphere is related to the variation of the structure of refractive index with time; i. e. the worst propagation conditions are likely to occur during

periods of extreme stratification of the atmosphere. On overland paths and in temperate climates, such conditions normally exist during the night and early morning hours of summer days. Reflections from rapid changes of the refractive index within a height range of several tens of meters above the surface of the earth can be a source of multi-path propagation.

For designing radio relay systems it is often necessary to predict the probability of outages due to deep fades for very small percentages of the time (i. e., on the order of 0.01 percent for an average hop of about 50 kilometers). If dual vertical space diversity or dual frequency diversity is used and fades on the two sets of equipment are not well correlated, prediction of the probability of the fade depth must be made for approximately 0.01 percent of the time. Although diversity aids in preventing outages caused by interference fading, outage time cannot be directly equated to depth and frequency of fading of the combined signal because multi-path causes distortion as well as attenuation. The fading depth exceeded for a small percent of the time increases with path length and increases slightly with frequency. Multi-path fading is also a function of the terrain near the path, the atmospheric conditions, and the angle of penetration through the atmosphere.

"Fades due to non-linear refractive index gradients (stratified atmospheric layers) are usually also of the multi-path, phase interference type, and can occur even when there are no reflections from terrain. A combination of ray paths caused by both ground and atmospheric layer reflections can produce very severe fading. Non-linear refractive index gradients are most likely to occur during the night, with light winds, clear skies, and high humidity near the surface"[7].

3-7 Radio Interference:

Interference from unwanted signals may be classified as either

external (from other systems or sources) or self-interference (within the system), the latter type can be controlled by good planning and equipment design, including route layout, since it is caused by equipment components within the proposed system, or overreach from adjacent or remote links due to unusual refractive index gradients, as is the case in the golf of Sirte. External interference (interference from other radio spectrum users) is most economically controlled in the planning stage by utilizing distance or terrain blockage for attenuating unwanted signals if their sources are known.

Overreach is self-interference caused by signals on the same frequency reaching one link from another in the same system. The scarcity of available spectrum space requires that an allocated frequency be used several times within one LOS system. If a ducting condition is present, links using the same frequency may be subject to mutual interference unless a combination of factors is sufficient to provide isolation between affected sites. Three of these factors are:

1- The way the links along the route are staggered

2- Terrain blockage.

3- Choice of path orientation, with antenna discrimination in the direction of the unwanted signal.

External interference, between 1 and 40 GHz, may come from any of several man-made sources such as harmonics from transmitters below 1 GHz, radar stations, or existing microwave communication systems, the tools for overcoming external interference are link orientation, distance, terrain blockage, antenna characteristics and polarization discrimination, band pass filters, and inter-organization consulting and cooperation. "Possible sources of unwanted signals within 100 kilometers of each

proposed site should be located and plotted on a map. The unwanted signals should then be investigated for potential interfering fundamental frequencies and harmonics, transmitter power, and antenna gain and polarization in the direction of the proposed site. Care must also be exercised to assure that the proposed system will not interfere with existing radio facilities"[7].

One common source of reflections is the ground. It tends to be more of a factor on paths in rural areas; in urban settings, the ground reflection path will often be blocked by the clutter of buildings, trees, etc. In paths over relatively smooth ground or bodies of water, however, ground reflections can be a major determinant of path loss. For any radio link, it is worthwhile to look at the path profile and see if the ground reflection has the potential to be significant. It should also be kept in mind that the reflection point is not at the midpoint of the path unless the antennas are at the same height and the ground is not sloped in the reflection region - just to remember the old maxim from optics that the angle of incidence equals the angle of reflection.

In a radio path consisting of a direct path plus a ground-reflected path, the path loss depends on the relative amplitude and phase relationship of the signals propagated by the two paths. In extreme cases, where the ground-reflected path has Fresnel clearance and suffers little loss from the reflection itself (or attenuation from trees, etc.) then, its amplitude may approach that of the direct path, depending on the relative phase shift of the two paths, we may have an enhancement of up to 6 dB over the direct path alone, or cancellation resulting in additional path loss of 20 dB or more. The difference in path lengths can be estimated from the path profile, and then translated into wavelengths to give the phase relationship. Then we have to account for the reflection itself. The

amplitude and phase of the reflected wave depend on a number of variables, including conductivity and permittivity of the reflecting surface, frequency, angle of incidence, and polarization.

"It is difficult to summarize the effects of all variables which affect ground reflections, but a typical case is shown in Fig. (3.7). This particular figure is for typical ground conditions at 100 MHz, but the same behavior is seen over a wide range of ground constants and frequencies. There is a large difference in reflection amplitudes between horizontal and vertical polarization (denoted on the curves with "h" and "v", respectively), and that vertical polarization in general gives rise to a much smaller reflected wave. However, the difference is large only for angles of incidence greater than a few degrees, these angles will only occur on very short paths, or paths with extraordinarily high antennas. For typical paths, the angle of incidence tends to be of the order of one degree or less - for example, for a 10 km path over a smooth earth with 10 m antenna heights, the angle of incidence of the ground reflection would only be about 0.11 degrees. In such a case, both polarizations will give reflection amplitudes near unity (i.e., no reflection loss), perhaps more surprisingly, there will also be a phase reversal in both cases. Horizontally-polarized waves always undergo a phase reversal upon reflection, but for vertically-polarized waves, the phase change is a function of the angle of incidence and the ground characteristics" [7]. The upshot of all this is that for most paths in which the ground reflection is significant (and no other reflections are present), there will be very little difference in performance between horizontal and vertical polarization, for very short paths, horizontal polarization will generally give rise to a stronger reflection, if it turns out that this causes cancellation rather than enhancement, switching to vertical polarization

may provide a solution, in other words, for shorter paths, it is usually worthwhile to try both polarizations to see which works better (of course, other factors such as mounting constraints and rejection of other sources of multi-path and interference also enter into the choice of polarization).

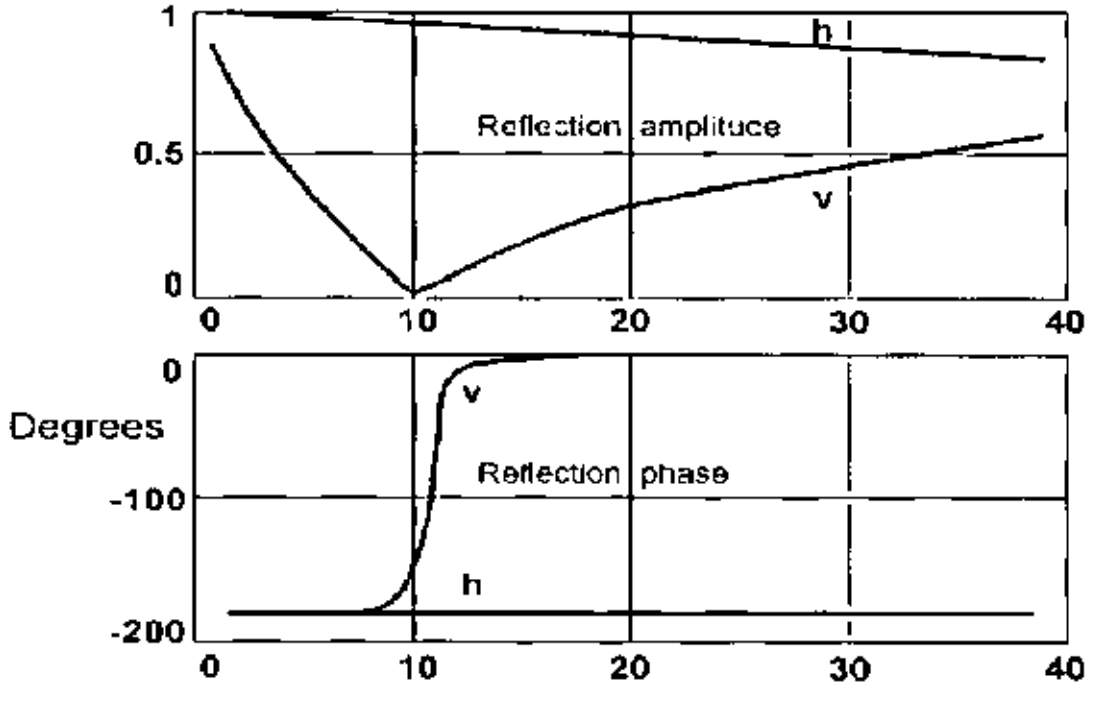

Figure (3.7) Typical Ground Reflection Parameters

As stated above, for either polarization, as the path gets longer we approach the case where the ground reflection produces a phase reversal and very little attenuation, at the same time, the direct and reflected paths becoming nearly more equal, the path loss ripples up and down as we increase the distance, until we reach the point where the path lengths differ by just one-half wavelength, combined with the 180° phase shift caused by the ground reflection, this brings the direct and reflected signals into phase, resulting in an enhancement over the free space path loss (theoretically 6 dB, but this will seldom be realized in practice). Thereafter, it's all downhill as the distance is further increased, since phase difference between the two paths approaches in the limit the 180°

phase shift of the ground reflection. In this region, the received power follows an inverse fourth-power law as a function of distance instead of the usual square law (i.e., 12 dB more attenuation when we double the distance, instead of 6 dB). The distance at which the path loss starts to increase at the fourth-power rate is reached when the ellipsoid corresponding to the first Fresnel zone just touches the ground. A reasonably good estimate of this distance can be calculated from the equation

$$d = \frac{4h_1h_2}{\lambda} \quad \text{..... (3-4)}$$

where h_1 and h_2 are the antenna heights above the ground reflection point. "Serious problems with ground reflections are most commonly encountered with radio links across bodies of water. Spread spectrum techniques and diversity antenna arrangements usually can't overcome the problems - the solution lies in sitting the antennas (e.g., away from the shore of the body of water) such that the reflected path is cut off by natural obstacles, while the direct path is unimpaired. In other cases, it may be possible to adjust the antenna locations so as to move the reflection point to a rough area of land which scatters the signal rather than creating a strong specular reflection"[7].

3-8 Other Sources of Reflections:

"The loss of LOS paths may sometimes be affected by weather conditions, rain , fog and dust (clouds) become a significant source of attenuation only when we get well into the microwave region, attenuation from fog only becomes noticeable (i.e., attenuation of the order of 1 dB or more) above 30 GHz, snow is in this category as well, rain attenuation becomes significant at around 10 GHz, where a heavy rainfall may cause

additional path loss of the order of 1 dB/km"[7].Sand and dust effects are the subject of this project and their effect will be investigated for Libya.

3-9 Diversity Measurements

For many years, radios on LOS paths have used diversity signals as a protection against the effects of multi-path fading, diversity signals are versions of the transmitted signal that are derived at the receiving site by a separate means. In space diversity, this second signal is obtained from a second receiving antenna on the same tower: in frequency diversity, it is obtained by transmitting the same signal over a different radio channel. Diversity improvements can be obtained by switching between the signals, or alternatively, in the case of space diversity, by combining them, while digital radios make use of both of these forms of diversity, they can also beneficially employ other forms of diversity. "Work over the last few years has established that either antenna pattern or angle diversity can be used to reduce the multi-path dispersion and the fade loss appearing at the receiver. These approaches to diversity are motivated by the cost benefits that are derived by using a second feed in a single antenna as a means of obtaining angle diversity, or by relieving the requirements of large antenna separations that have been required for the application of space diversity in analog systems. Large separations require tower modifications"[5].

"Another form of diversity, that is available to digital but not to analog, systems, is polarization diversity, polarization diversity, is not used so much as a fading countermeasure, but as a means of increasing the carrying capacity of a given radio frequency channel. Digital radios that use both polarizations effectively double the capacity of a channel assignment on a link"[5] .

3-9-1 Space Diversity:

"Figure (3.8) shows time-faded-below distributions derived from an experiment that monitored propagation during a one month period. The main antenna was a 10 foot (3m) pyramidal Horn reflector antenna; the diversity antenna was a 3 meter dish located 8.5 m below. Receiver power in a 6 GHz channel was monitored on both at 12 frequencies equally spaced at 2.2 MHz across the band (24.2 MHz bandwidth)"[5].

All of the distributions in Figure (3.8) were developed from two curves that represent the single frequency fading on the two antennas, there is about 50% more fading on the horn than on the dish, such differences in fade time in a month of observation are neither unusual nor significant. Immediately below these two distributions is the distribution of the least faded signal. This is the single frequency fading that would be observed if the two signals had passed through an ideal switch. The least-faded distribution falls off twice as rapidly as the non diversity distributions for deep fades. The difference (ratio) between this distribution and the one for the main antenna is denoted as the improvement factor at that fade level, for instance, the fade time at the 30 dB level is 12 times as large for the non diversity signal as for the diversity signal thus, an FM system with a 30 dB fade margin would experience 12 times less fading at the critical level by operating with switched diversity. A widely used formula for this improvement factor is

$$I_s = 1.2 \times 10^{-3}\, S^2\, (f/d)\, 10^{(A-V)/10} \qquad \ldots\ldots\ldots\ldots\ldots\ldots\ldots\ldots\ldots\ldots (3\text{-}5)$$

Where : A is the fade depth (dB), S is the vertical separation of receiving antennas (m), center-to-center $(5 \leq S \geq 15)$, f is the frequency (GHz) $(2 \leq f \leq 11)$, d is the path length (km) $(24 \leq d \leq 70)$, and $V = |G_1 - G_2|$, where G_1 and G_2 are the gains of the two antennas [5].

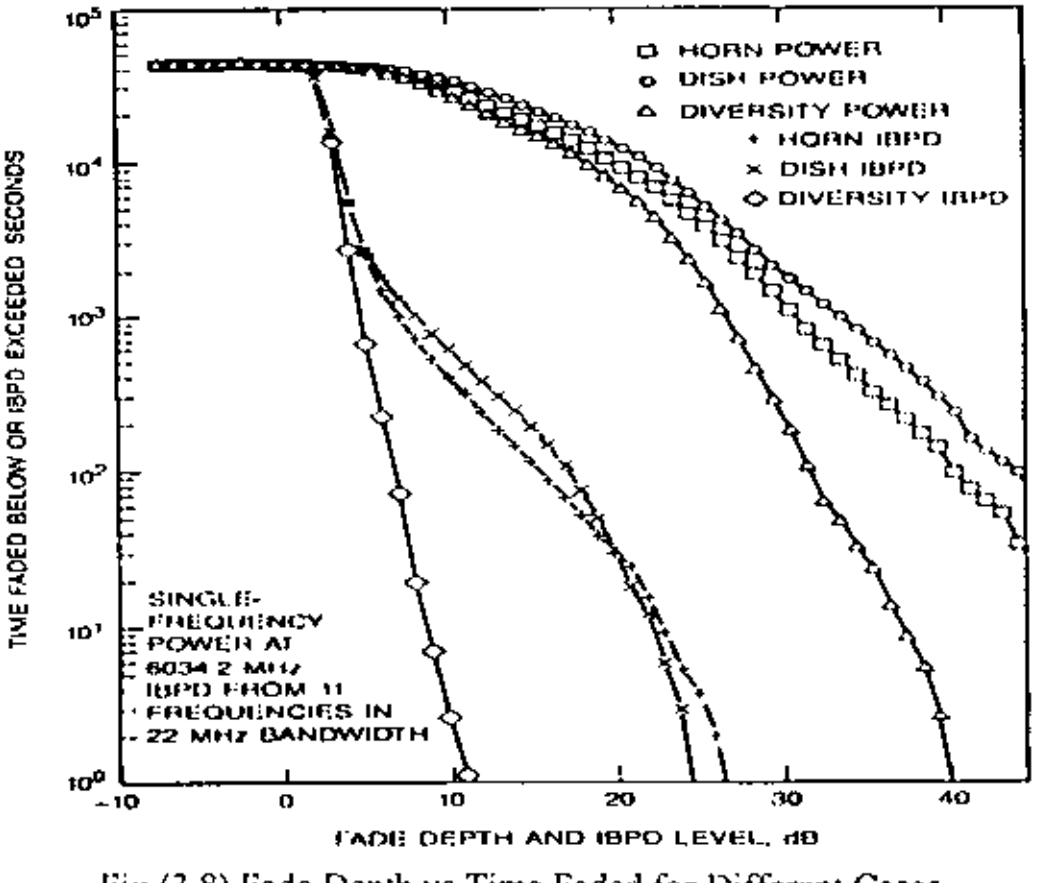

Fig.(3.8) Fade Depth vs Time Faded for Different Cases

The In-Band Power Difference (IBPD) distribution for the experimental period is also shown in Figure (3.8), except, that the third distribution is, in this case, the least dispersive (smallest IBPD). This is the IBPD distribution that would be observed at the output of an ideal dispersion avoidance switch. Because the BER of a digital radio correlates well with the occurrence of IBPD, the difference between the diversity and non diversity IBPD distributions can also be viewed as an improvement factor. Thus, we see that a system that could withstand (on the average) 10 dB of IBPD would have experienced 450 seconds of outage in a non diversity configuration, but only about 3 seconds with switched diversity. There are, at present, no agreed formulas for predicting the dispersion improvement factor, or dispersion occurrence factor (dispersion ratio) for that matter. However, the dispersion

improvement factor is often viewed as being insensitive to antenna spacing, except at smaller spacing where some studies that it may improve [5].

3-9-2 Frequency Diversity:

"Although frequency diversity protection has been used with FM systems for many years, there have been few reports of experimental observations of its potential for improving the performance of digital radios, this results, in part, from the smaller single-frequency improvement factors that are obtained for reasonable frequency separations, the improvement factor for frequency diversity is given by :

$$I_f = (\frac{0.8}{fd})(\frac{\Delta f}{f})10^{\frac{A}{10}} \quad \text{..... (3-6)}$$

Where:

f is the band center frequency (GHz) ($2 \leq f \leq 11$)

d is the path length (km) ($30 \leq d \leq 70$)

($\Delta f/f$) is the relative frequency spacing as a percentage

and A is as defined in (3-5) .

Equation (3-6) can be used for values of ($\Delta f/f$) up to 5%, it was derived originally from propagation measurements that support its use up to values of at least 10%, thus, for channels in the 6 GHz band separated by 60 MHz, the improvement for a 40 km path would be limited to a factor of about 3 at 30 dB.

3-9-3 Cross-Polarized Channels :

Radio links carrying several channels use both horizontal and vertical polarizations, with adjacent channels usually cross-polarized to minimize interference, Co-channel cross-polarized operation uses both

polarizations in a given channel bandwidth. One must describe the transmission for either a horizontally or vertically polarized signal to a receiver with the same or crossed polarization.

"Measurements of this type have been performed; however, because of the difficulties of presenting the results, they have only been analyzed from a modeling viewpoint. For an ideal system operating under ideal conditions, the cross-transfer functions would be zero. That is, energy transmitted horizontally (vertically) would not reach the receiver using vertical (horizontal) polarization. Imperfections in the antennas and waveguides determine the lower bound on this cross coupled energy. Atmospheric conditions, notably rain and ground reflections, can also contribute to this cross coupling. Frequency selective fading is the most complex and variable mechanism for introducing coupling, and this combination produces the most damaging effect. Most cross-polarization experiments monitor cross-polarization discrimination (XPD), which for a given transmitted polarization, is the ratio of the power received on the same polarization to that received on the cross polarization. In the past, such measurements were made on a narrow band, or single-frequency basis; for digital systems, they have also been made on a wideband basis using the broadband digital signal, the statistics of such measurements taken simultaneously" [5].

3-10 Rain Attenuation:

Rain is one of the most significant atmospheric phenomenon which can affect the propagation of microwave signals on LOS paths. However, we do not mean to say that there are no other effects. At frequencies above 20 GHz, molecular absorption due to water and oxygen can be important, but the frequency bands allocated to terrestrial microwave service tend to avoid these absorption lines. Other atmospheric effects,

such as losses due to sand or dust storms, are usually not considered this because most of the work was done in areas were there is no sand or dust storms.

"The plots of Figure (3.9) are for spherical raindrops. Real raindrops are somewhat flattened (sometimes canted) from their interaction with the atmosphere. Because of this flattening, a raindrop will have a smaller size in the vertical than in the horizontal dimension. Consequently, the attenuation of a horizontally polarized wave will be larger than that of a vertically polarized wave"[5].

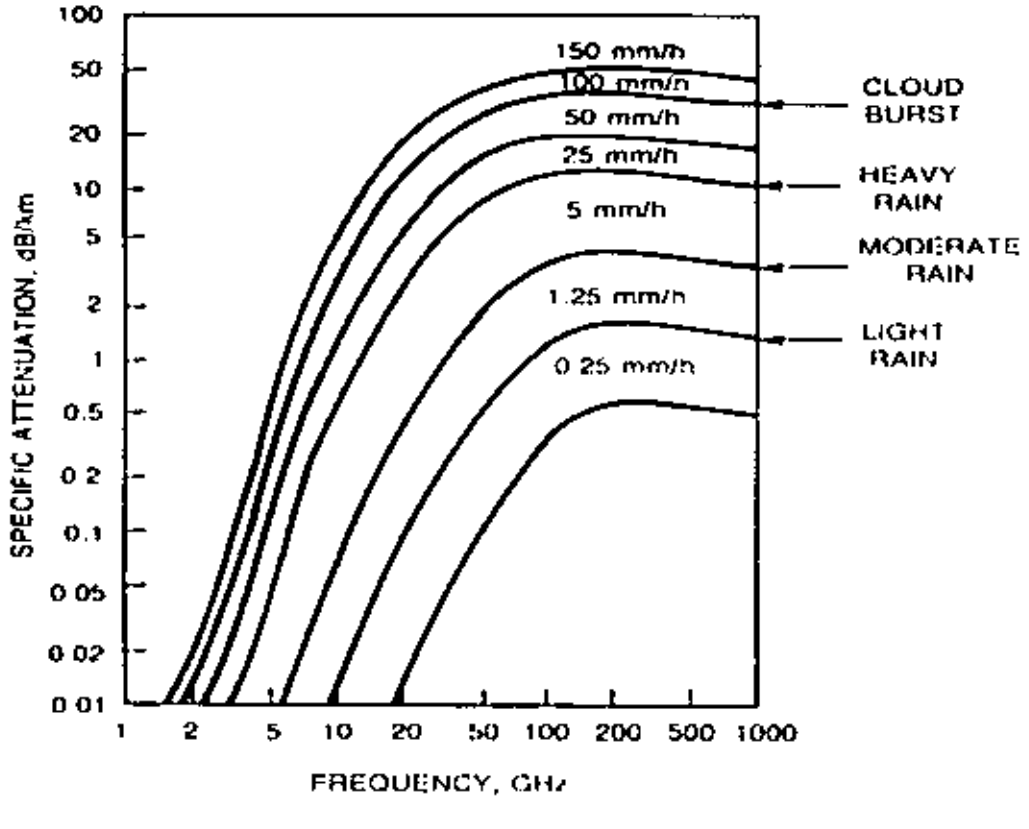

Fig.(3.9) Specific Attenuation Due to Rain

The sand and dust suspended particles could have an effect on the microwave signal, this is what will be studied in this project.

CHAPTER 4

Samples Collection and Meteorological Data

4-1 Introduction

This chapter will be devoted to presenting the metallurgical, the sand and dust samples collected along with chemical and dimension wise analysis

Wind storms will make the sand and dust particles be removed from their places, if it is strong enough the particles will climb as high as tens of meters and this is dependent on the wind speed and the properties of the land and the surroundings regions, there has been reports of a dust as high as 1000 meters, in Libya sudden storms usually happen on a short notice with wind speed recorded of around 50 km/h.

The wind is a vector quantity with magnitude and direction, it is standard that the speed of wind be measured at an altitude of ten meters above the sea level with the direction of the wind as the direction from which it is coming not the direction to which it is going .The direction of the wind is represented by the clock wise direction as represented in Figure (4.1).

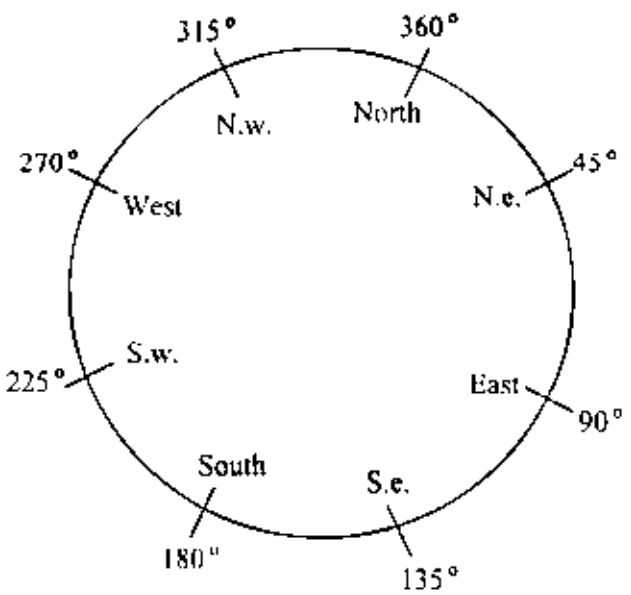

Fig. (4.1)Standard Wind Directions Reference

4-2 The Data of Dust and Sand Storms:

The collage meteorological data obtained for a period of 14-years (from 1990 up to the end of 2003) from two recording stations near to the path of the first part of the great man made river , this is to find the speed and direction of the wind for that area as in tables (4-1) and (4-2) [8]. In these tables the first number stands for the direction from which the wind is coming, while the second stands for the speed in knot (*1 knot= 1.85 km/h*).

In this thesis sand and dust samples were collected from seven places (stations) along the microwave link as shown in Table (4-3). The first is Agedabia which is near the Mediterranean sea (in the golf of Sirte) but has a climate as that for the desert besides, the high humidity, the second is Jalo, which is deep in the desert (about 250 km to the sought of the sea side), also we used five other sites, four of them located between Agedabia and Jalo and the fifth one in Serier deep in the desert and the fifth is to the east of Jalo Fig. (4.2).

In Agedabia the fastest storm reached a speed of 38 knots and it was recorded at three times on the years 1996(Apr.), 1997(Apr) and 2000(Dec). In Jalo the fastest storm reached a speed of 42 knots and it was recoded on May. 1994. From Table (4-1) and Table (4-2) we notice that the biggest storms are over the period from Feb. to May, and then it peaks again in Dec. The recorded data lacks information about the visibility we failed to find any recorded data relating to the Libyan area however we did measure the visibility of the dust storm which happened on 24/2/2006 when this study is in progress, it was found 100m at a wind speed of 30 Knots, and it will be used to estimate the visibility based on the assumption that the visibility is inversely proportional to the wind

speed assuming no other affecting factor or all other factors stay the same.

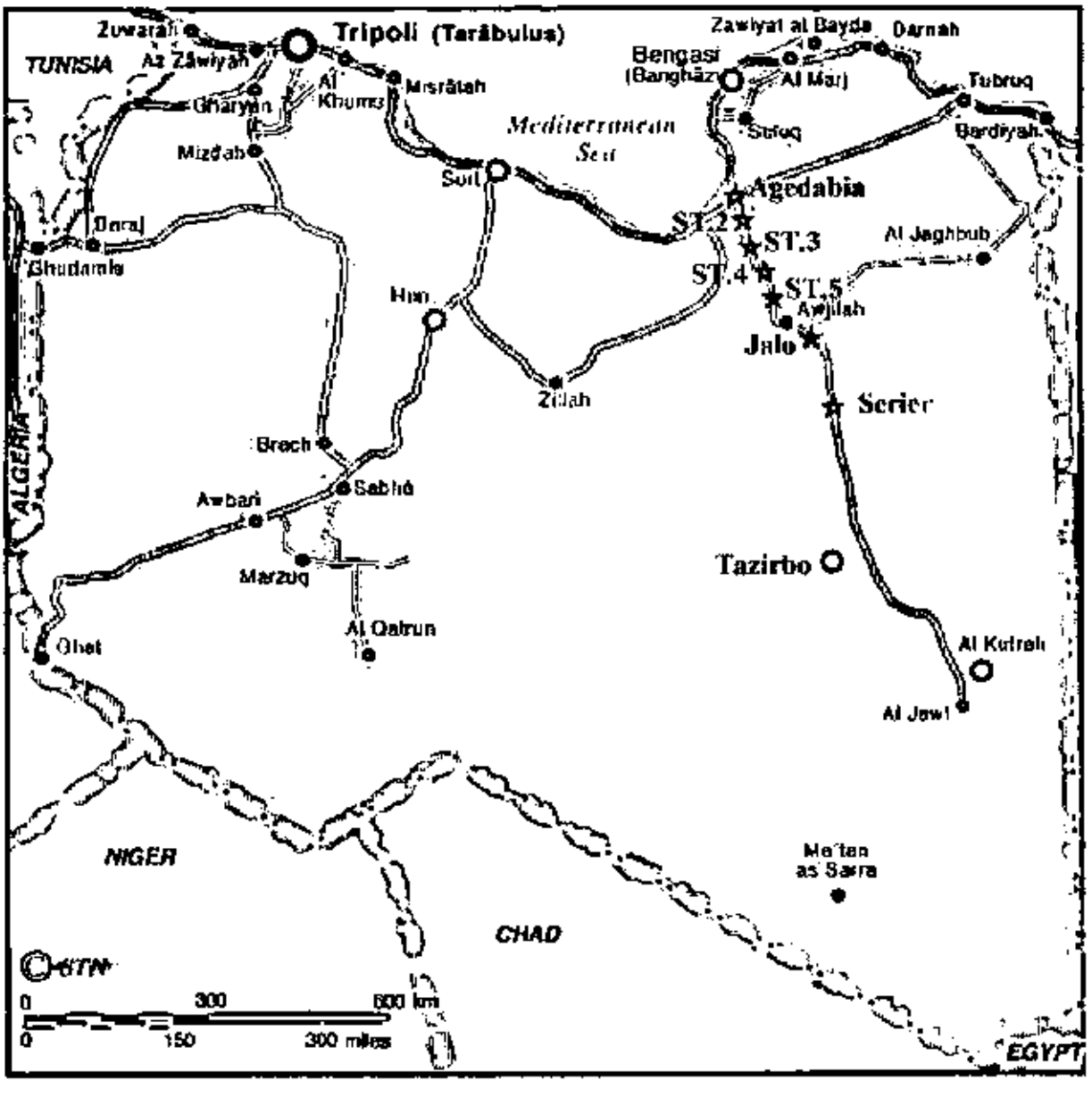

Fig. (4.2) Map Showing the Cites from Which Data is Collected

Table (4-1) Wind Speed for Agedabia

MAXIMUM WIND SPEED (Knots)												
STATION NAME & NO. : AGEDABIA 62055												
PERIOD: (1990-2003) LAT. 30-43 N LON. 20-10 E ELV. 70 M												
YEAR	JAN	FEB.	MAR	APR	MAY	JUN.	JUL	AUG	SEP	OCT.	NOV	DEC
1990	120/27	330/20	180/20	330/20	090/20	170/20	350/20	330/20	350/20	090/18	060/23	300/29
1991	300/21	090/22	090/32	330/24	160/27	340/19	310/20	350/20	330/15	340/21	030/18	330/24
1992	090/15	330/20	110/34	160/23	090/35	100/18	330/20	330/22	330/20	160/19	330/14	160/20
1993	270/13	060/17	300/22	330/18	110/18	300/18	300/22	340/18	160/20	170/20	120/18	330/16
1994	330/23	170/20	350/18	140/25	360/22	330/17	330/20	330/22	330/18	200/23	200/15	300/20
1995	270/23	330/15	180/20	220/22	180/20	110/18	350/19	330/21	360/20	360/18	120/18	270/15
1996	140/27	270/25	330/26	350/38	160/25	070/23	330/22	360/20	180/20	160/20	330/20	320/25
1997	330/28	360/30	180/26	300/30	090/30	360/23	360/24	330/23	330/22	180/25	160/20	310/38
1998	300/20	020/20	120/26	180/27	330/25	360/20	360/21	360/18	330/22	360/22	300/20	180/25
1999	120/20	120/23	180/28	160/28	330/20	350/20	360/20	360/20	360/20	360/18	090/25	330/22
2000	160/20	350/20	360/25	360/38	180/25	350/28	360/22	360/22	180/20	160/20	360/26	360/18
2001	180/25	310/30	360/20	270/23	350/30	350/20	360/23	360/20	180/20	360/18	180/20	270/22
2002	360/20	360/28	360/28	240/35	180/26	350/23	360/25	360/25	090/23	240/18	320/22	300/18
2003	360/20	360/27	160/30	180/25	350/25	150/22	030/20	360/20	360/22	360/14	320/20	180/25

Table (4-2) Wind Speed for Jalo

MAXIMUM WIND SPEED (Knots)												
STATION NAME & NO. : JALO 62161												
PERIOD: (1990-2003) LAT. 29-02 N LON. 21-34 E ELV. 60 M												
YEAR	JAN	FEB.	MAR	APR	MAY	JUN.	JUL	AUG	SEP	OCT.	NOV	DEC
1990	300/21	270/16	360/17	290/25	330/20	160/19	360/15	330/14	260/15	200/19	140/25	280/19
1991	290/18	300/22	120/25	180/24	320/25	350/12	340/12	360/12	190/15	360/18	140/15	280/23
1992	280/16	280/20	280/30	180/28	310/19	140/18	350/11	340/11	330/14	160/13	310/22	170/20
1993	290/12	280/20	320/23	360/18	220/29	330/15	340/16	320/13	190/17	120/10	170/15	270/18
1994	270/30	290/20	330/22	120/29	300/42	330/16	330/12	330/15	330/10	340/12	070/15	260/15
1995	220/15	340/20	170/30	270/21	240/20	330/17	340/20	180/15	170/20	180/20	190/18	180/18
1996	190/20	270/38	350/20	180/30	120/20	360/18	340/20	360/20	180/20	330/18	190/18	270/20
1997	320/18	350/25	360/30	340/33	330/18	350/20	340/24	270/20	360/20	350/25	180/25	280/24
1998	220/18	290/18	190/30	170/20	350/25	350/20	350/20	360/16	200/17	190/20	170/20	360/20
1999	290/20	270/25	170/20	170/27	320/25	350/19	360/20	360/15	350/20	360/20	170/20	330/20
2000	340/18	210/20	270/25	330/35	150/35	350/22	350/20	360/20	170/23	180/20	330/18	180/20
2001	270/25	330/25	180/28	180/27	330/32	350/15	360/20	190/20	240/19	350/18	300/25	270/30
2002	210/22	300/24	300/27	160/25	360/27	350/28	330/20	360/18	180/20	300/18	170/20	240/20
2003	200/20	300/32	260/26	150/30	330/26	350/20	360/20	350/16	100/20	350/14	360/20	210/18

4-3 The Microwave link from Agedabia to Jalo :

- The microwave link is an analog system and it is operating at a frequency of 3 GHz.

- This link has six stations from Agedabia (Station 1) to Jalo .

- Station 2 to the south of station 1 (Agedabia) about 20 Km with tower height of 82 m.
- Station 3 diverge from station 2 about 55 Km and the height of the tower 92 m.
- Station 4 diverge from station 3 about 55 Km and the height of the tower 92 m.
- Station 5 diverge from station 4 about 45 Km and the height of the tower 82 m.
- Station 6(Ojala) diverge from station 2 about 55 Km and the height of the tower 92 m.

We collected the sand and dust samples from four sites and collect the sand samples from Serier, Jalo and Agedabia.

The dust samples are required to be collected at a height of 2m, and know such place available from which we could have collected the dust.

4-4 Samples of Dust and Sand:

The samples were collected in the spring of 2006, the dust was collected from a height of 2m from the surface of earth (above the roofs of the stations) ,but the sand collected from that laying on objects on surface of the ground of the stations, The samples were collected from the sites are given in Table (4-3) along with the collection dates.

Table (4-3) Place and Type of Sample

S. No.	Type	Region of samples	Data
1	Sand	Serier (after Jalo about 150Km to south)	29/03/2006
2	Sand	Jalo city	29/03/2006
3	Sand	Agedabia station	16/05/2006
4	Sand	Station 2	16/05/2006
5	Dust	Station 2	16/05/2006
6	Sand	Station 3	16/05/2006
7	Dust	Station 3	16/05/2006
8	Sand	Station 4	16/05/2006
9	Dust	Station 4	16/05/2006
10	Sand	Station 5	16/05/2006
11	Dust	Station 5	16/05/2006

The given samples are the results of accumulation over a period of time but the rate of accumulation is not known to use, there is no way to know it , and it is not easy to predict. To collect data on a stormy day one has to prepare a collecting object and have it ready and move to the storm site on a short notice, these storms happen on a short notice and do not last long, we believe that what we did in collecting the data is the best under the Libyan conditions and can be considered as a start for a full scale project.

4-5 Analysis of the samples:

The analysis of these samples were done in two laboratories , one in the *Libyan Iron and Steel Company* (LISCO) in Misurata, and the second in the *Libyan Petroleum Institute* in Tripoli. These are the only two places that have an equipments that is capable to carry some of the analysis we were looking for which mainly the chemical composition, the PSD, the conductivity, the density, ration of the major to minor axis and the permeability. We managed only to have, the chemical composition

analysis, the particle size distribution, the density and the conductivity. We hopped to be able to find the relative permittivity and relative permeability of the compound from direct measurements we could not so we will assume relative permeability one and estimate the permittivity using empirical equation and permittivity of the constituents of the compound of each sample.

4-5-1 Libyan Iron and Steel Company Analysis:

I- Chemical Composition:

The chemical composition analysis was carried out on samples from the sand of Serier and Jalo (samples 1 and 2), with the results presented in Table (4-4) and table (4-5) respectively. From the two tables we see that more than 87% silicon oxide with the metal oxides not more than 4.8%.

The chemical composition of other samples as determined by the Libyan Iron and Steel Company laboratory are given in Tables (4-6) & (4-7)and (4-8), it is worth noticing that the results in Tables (4-6) &(4-7) and (4-8) shows that samples do not have the following metal oxides in their composition (TiO_2 , ZrO_2 , P_2O_5 , MnO) , again these samples are mainly made from silicon oxide, for samples 2,3,10 but a big drop in the silicon oxide percentage on samples 4,5,6. The four samples have a close percentage of the other main metal oxide. Tables (4-7) and (4-8) shows also the practical size distribution (PSD) with the diameter of the particles raging from less than 0.15mm to 1.2mm.

Table (4-4) Libyan Iron and Steel Analysis/ sample (1)

Sample Sand "Sarir" – No "01" - 29/03/2006			
Oxide	**Mass %**	**Element**	**Mass %**
SiO2	90.30	Si	42.22
Al2O3	4.15	Al	2.20
CaCO3	1.68	Ca	1.20
KCl	1.62	K	0.85
NaCl	1.15	Na	0.58
MgCO3	0.752	Mg	0.453
SO3	0.489	Sx	0.196
Fe2O3	0.363	Fe	0.254
TiO2	0.0835	Ti	0.0501
P2O5	0.0711	Px	0.031

Table (4-5) Libyan Iron and Steel Analysis/ sample (2)

Sample Sand "Jalo" – No "02" - 29/03/2006			
Oxide	**Mass %**	**Element**	**Mass %**
SiO2	87.99	Si	41.14
Al2O3	4.85	Al	2.57
CaCO3	3.50	Ca	2.50
KCl	1.818	K	0.952
MgCO3	0.709	Mg	0.428
Fe2O3	0.708	Fe	0.495
NaCl	0.864	Na	0.340
TiO2	0.241	Ti	0.145
ZrO2	0.221	Zr	0.164
P2O5	0.0711	Px	0.031
MnO	0.0203	Mn	0.0157

Table (4-6) Libyan Iron and Steel Analysis / four samples

Sample No.	SiO_2	CaO	MgO	Fe_2O_3	Al_2O_3
4	66.91	22.40	1.08	4.43	2.15
5	31.48	48.86	1.63	4.20	1.68
6	58.07	33.68	1.18	4.02	1.00
10	91.10	4.17	0.20	3.10	1.50

II- Particle- Size Distribution (PSD) :

From the analysis for the PSD of two samples (Samples 2 and 3). Sample number 2 has 51% (by weight) of it with diameter less than 0.15mm , while sample number 3 has 56% of it with diameter equal to 0.15mm .Tables (4-7) and (4-8) .

Table (4-7) Libyan Iron and Steel Analysis/ sample (2)

Sample No.	SiO_2	Al_2O_3	$CaCO_3$	$MgCO_3$	KCl	NaCl	Fe_2O_3
2	84.69	6.89	2.83	1.07	2.12	2.15	0.454

Sample No.	1.2mm	0.85mm	0.6mm	0.4mm	0.15mm	<0.15	SUM
2	2.00g	2.3g	10.6g	28.2g	446.5g	515.3g	1004.9
%	0.20	0.23	1.05	2.81	44.43	51.28	100.00

Table (4-8) Libyan Iron and Steel Analysis/ sample (3)

Sample No.	SiO_2	Al_2O_3	$CaCO_3$	$MgCO_3$	KCl	NaCl	Fe_2O_3
3	38.93	6.07	49.54	1.46	1.43	1.02	1.29

Sample No.	1.2mm	0.85mm	0.6mm	0.4mm	0.15mm	<0.15	SUM
3	1.9g	24.6g	95.5g	157.9g	604.8g	180.0g	1064.7
%	0.18	2.31	8.97	14.83	56.80	16.91	100.00

III- Density and Conductivity:

The conductivity and density results for six samples are shown in the following table

Table (4-9) Libyan Iron and Steel Analysis

Sample No.	Desnsity (g/cm^3)	Conductivity (ms)
2	1.49	240
5	1.53	797
6	1.11	6.54
7	1.62	1660
8	1.72	90
9	1.57	565

4-5-2 Libyan Petroleum Institute Analysis:

I- chemical composition and Conductivity:

In the Libyan Petroleum Institute the analysis for five samples where conducted but the laboratory results came out as separate elements and only one in oxide form Table (4-10) . In the nature these elements exist in their oxide not separate form.

Table (4-10) Libyan Petroleum Institute

Sample No.	$Si(O)_2$(%)	Ca^{++}(%)	Mg^{++}(%)	Na^{+}(ppm)	K^{+}(ppm)	Cl(ppm)	Fe(ppm)	Conductivity (µmhos/cm)
2	95.373	1.042	0.0926	37	4.5	92	1685.2	169 (23.4)
9	83.673	3.820	0.206	31	6	63	6890.6	195.1(23.3)
8	90.525	3.047	0.158	7	2.5	23	1664.4	24.3 (23.2)
6	57.067	2.815	1.913	3.5	1	16	918.05	33.3 (23.2)
5	52.80	3.060	1.991	55	10	101	8772.6	260 (23.0)

A quick look to the results given the previous tables we see that there is a big difference between them and there is no way for use to find which center is accurate so we will work with the average of the two .The same difference occurs when we consider the particle size distribution .

II- Particle- Size Distribution (PSD) :

In the particle size distribution analysis, samples were analyzed and the results given in Tables (4-11) to (4-15).

Table (4-11) PSD of sample (2)

Sample(2) weight: 156.6 g **(sand sample)**

Screen opening (μm)	Weight (g)	Cumulative weight (g)	Weight %	Cumulative weight %
850	3.36	3.36	2.14559387	2.14559387
600	13.21	16.57	8.43550447	10.58109834
425	27.52	44.09	17.5734355	28.15453384
355	14.41	58.5	9.20178799	37.35632184
300	19.33	77.83	12.3435504	49.69987229
212	31.65	109.48	20.210728	69.91060026
180	9.1	118.58	5.8109834	75.72158365
150	9.98	128.56	6.37292465	82.0945083
125	7.81	136.37	4.98722861	87.08173691
90	12.64	149.01	8.0715198	95.15325671
75	3.36	152.37	2.14559387	97.29885057
32	4.1	156.47	2.61813538	99.91698595
25	0	156.47	0	99.91698595

59.3295 FU-ML 59.32% of the sample is between (212-425 μm) which is fine lower to medium lower sand

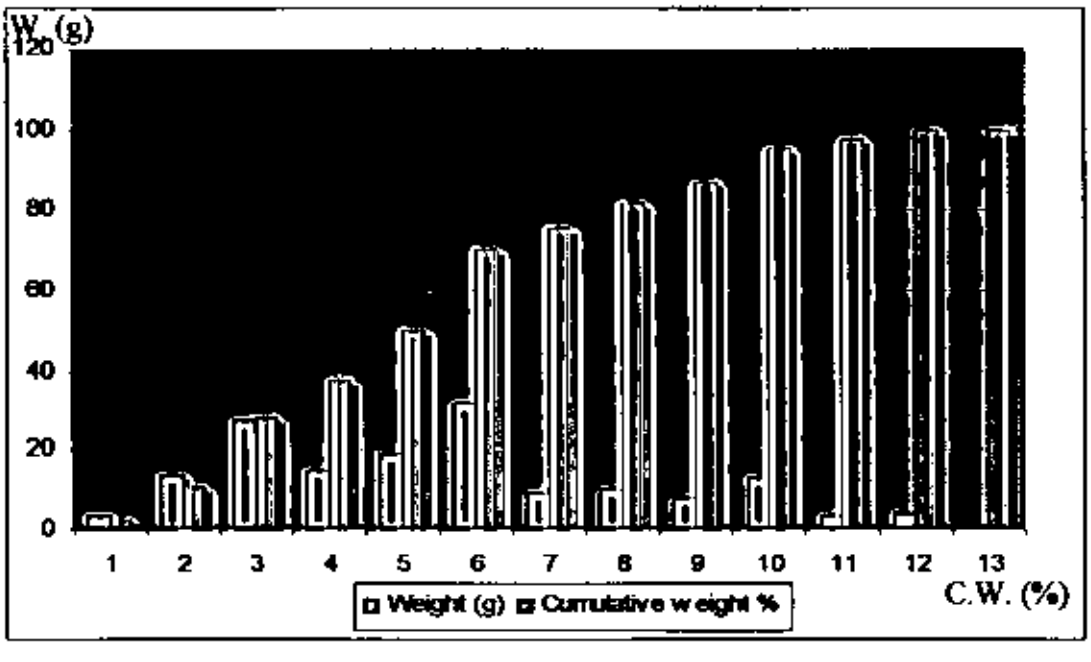

Fig. (4.3) Graph Between the Weight and Radii of Sample (2)

Table (4-12) PSD of sample (9)

Sample(2) weight: 58 g **(dust sample)**

Screen opening (µm)	Weight (g)	Cumulative weight (g)	Weight %	Cumulative weight %
850	0	0	0	0
600	0	0	0	0
425	0.1	0.1	0.17241379	0.172413793
355	0.28	0.38	0.48275862	0.655172414
300	0.01	0.39	0.01724138	0.672413793
212	6.31	6.7	10.8793103	11.55172414
180	3.24	9.94	5.5862069	17.13793103
150	5.53	15.47	9.53448276	26.67241379
125	14.1	29.57	24.3103448	50.98275862
90	15.32	44.89	26.4137931	77.39655172
75	4.31	49.2	7.43103448	84.82758621
32	6.68	55.88	11.5172414	96.34482759
25	0.6	56.48	1.03448276	97.37931034

50.72414 VF

50.72% of the sample is between (90-125 µm) which is very fine grained sand

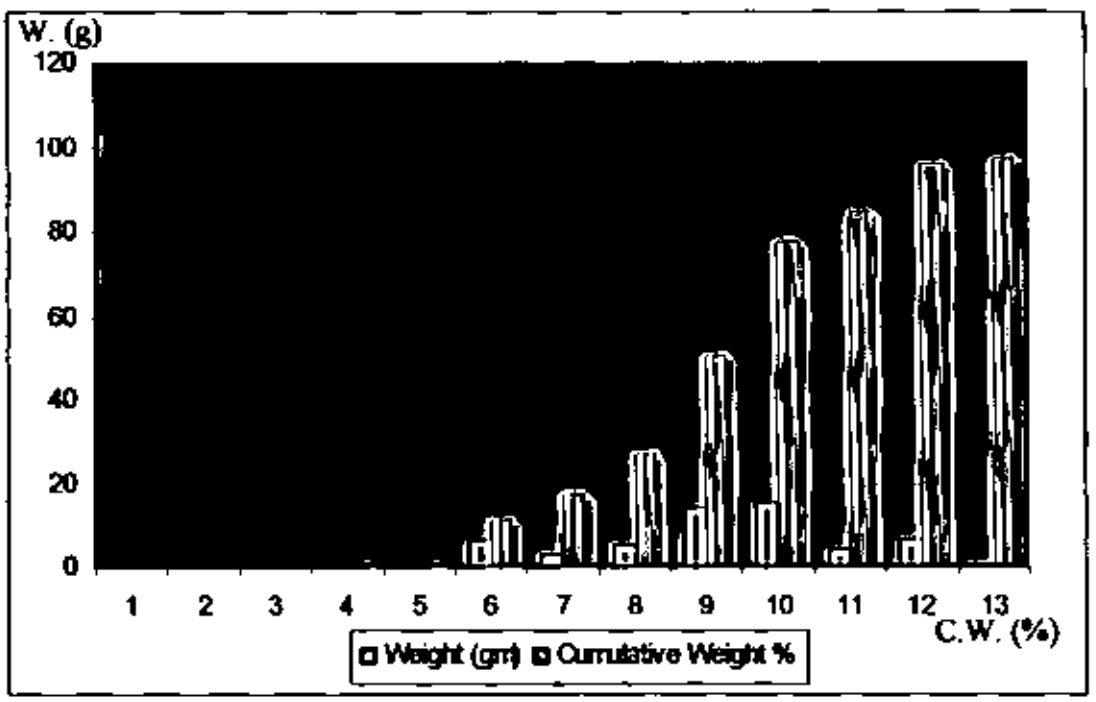

Fig. (4.4) Graph Between the Weight and Radii of Sample (9)

Table (4-13) PSD of sample (8)

Sample(Z) weight: 264.2 g **(sand sample)**

Screen opening (μm)	Weight (g)	Cumulative weight (g)	Weight %	Cumulative weight %
850	1	1	0.37850114	0.37850114
600	2.23	3.23	0.84405753	1.222558672
425	20.56	23.79	7.78198335	9.004542018
355	26.2	49.99	9.91672975	18.92127177
300	52.46	102.45	19.8561696	38.77744134
212	102.11	204.56	38.6487509	77.42619228
180	20.52	225.08	7.7668433	85.19303558
150	21.44	246.52	8.11506435	93.30809993
125	9.73	256.25	3.68281605	96.99091598
90	6.71	262.96	2.53974262	99.5306586
75	1.06	264.02	0.4012112	99.9318698
32	0.52	264.54	0.19682059	100.1286904
25	0	264.54	0	100.1286904

68.42185 FU-M 68.42% of the sample is between (212-355 μm) which is fine upper to medium grained sand

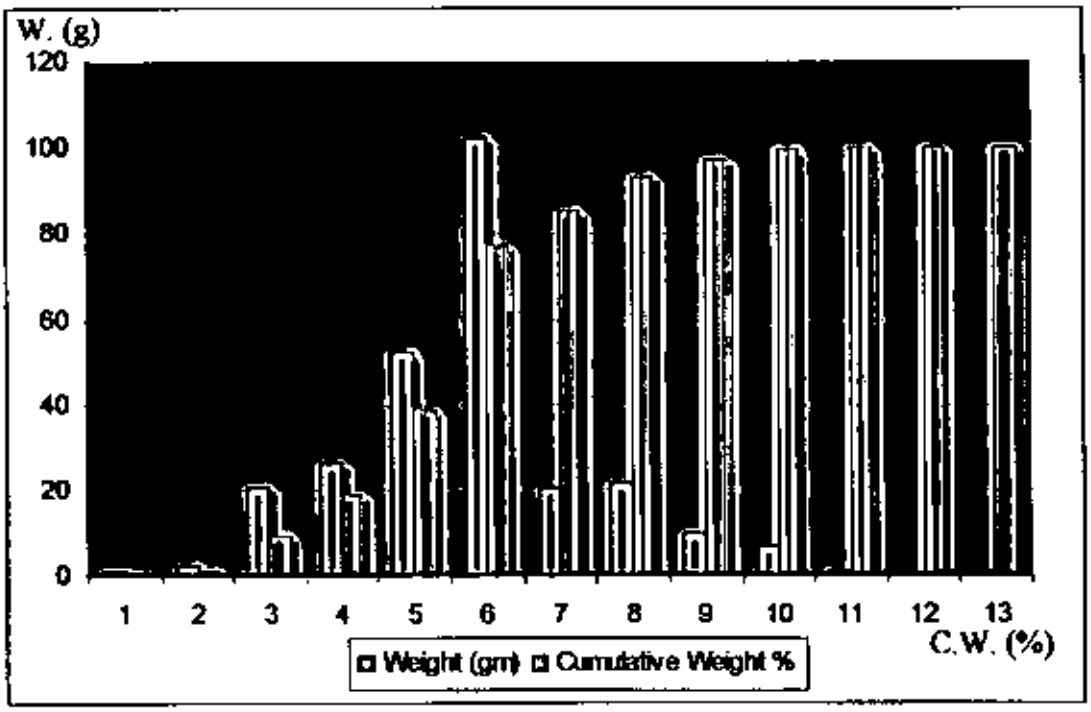

Fig. (4.5) Graph Between the Weight and Radii of Sample (8)

Table (4-14) PSD of sample (6)

Sample(2) weight: 311.3 g **(sand sample)**

Screen opening (μm)	Weight (g)	Cumulative weight (g)	Weight %	Cumulative weight %
850	6.07	6.07	1.94988757	1.94988757
600	42.91	48.98	13.7841311	15.73401863
425	28.36	77.34	9.1101831	24.84420174
355	27.26	104.6	8.75682621	33.60102795
300	30.26	134.86	9.72052682	43.32155477
212	58.17	193.03	18.6861548	62.00770961
180	23.01	216.04	7.39158368	69.39929329
150	20.29	236.33	6.51782846	75.91712175
125	10.43	246.76	3.35046579	79.26758754
90	5.93	252.69	1.90491487	81.17250241
75	1.3	253.99	0.4176036	81.59010601
32	3.82	257.81	1.22711211	82.81721812
25	51.25	309.06	16.4632188	99.28043688

73.96723 FL-CL 73.96% of the sample is between (150-600 μm) which is fine lower to coarse lower sand

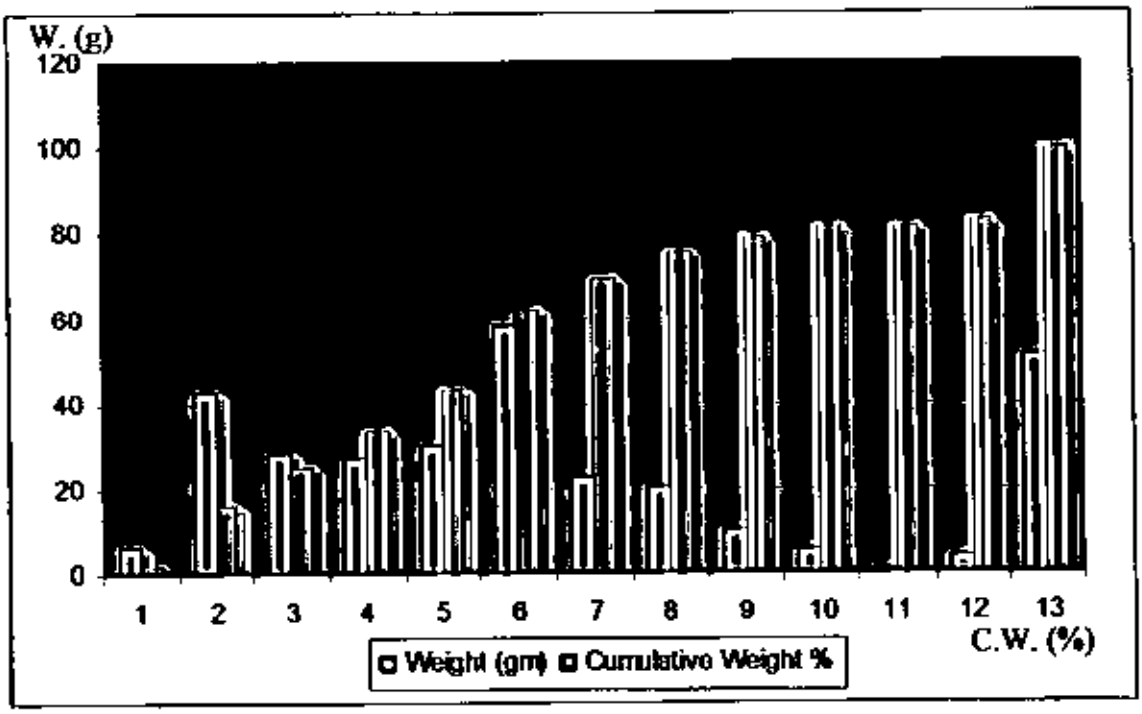

Fig. (4.6) Graph Between the Weight and Radii of Sample (6)

Table (4-15) PSD of sample (5)

Sample(2) weight: 53.6 g **(dust sample)**

Screen opening (μm)	Weight (g)	Cumulative weight (g)	Weight %	Cumulative weight %
850	0	0	0	0
600	0	0	0	0
425	0.18	0.18	0.3358209	0.335820896
355	0.11	0.29	0.20522388	0.541044776
300	0.22	0.51	0.41044776	0.951492537
212	1	1.51	1.86567164	2.817164179
180	0.78	2.29	1.45522388	4.27238806
150	1.73	4.02	3.22761194	7.5
125	3.24	7.26	6.04477612	13.54477612
90	16.94	24.2	31.6044776	45.14925373
75	8.71	32.91	16.25	61.39925373
32	19.55	52.46	36.4738806	97.87313433
25	1.15	53.61	2.14552239	100.0186567

84.32836 SLT-VF 84.32% of the sample is between (32-90 μm) which is silt to very fine sand

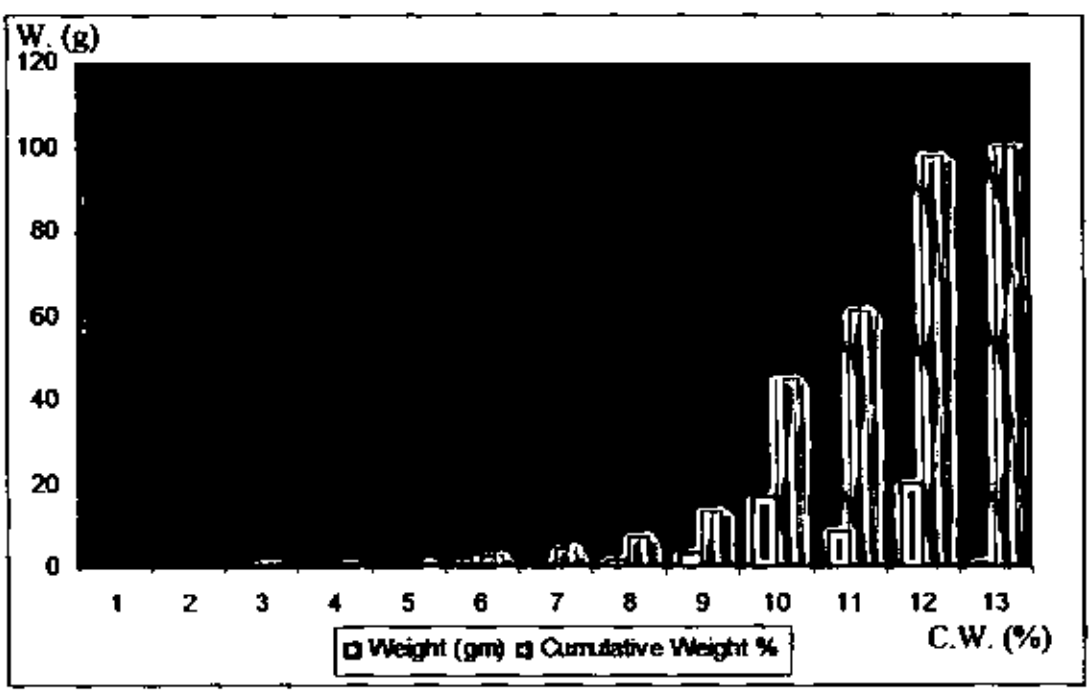

Fig. (4.7) Graph Between the Weight and Radii of Sample (5)

The results presented in this chapter are given in Appendix A "picture copy" we will analysis these results in the following chapter.

CHAPTER 5

Analysis of the Results

5-1 Introduction:

In this chapter results presented in chapter four will be analyzed, by finding the complex relative permittivity, the visibility, the dust and sand particle dimensions from these data one can estimate the different effects on the microwaves signal like the attenuation and scattering

5-2 Calculation of the Dielectric Constant for the Component:

From the values of the dielectric constant for the pure component, we can calculate the dielectric constant of the composite component by using the Looyenga equation as given by [9].

$$\epsilon_r^{1/3} = \sum_i \epsilon_i^{1/3} V_i \text{ ---------- (5-1)}$$

Where:

ϵ_r is the complex dielectric constant of the mixture.

ϵ_i is the complex dielectric constant of the i^{th} substance.

V_i is the relative volume of the i^{th} sample from the volume of the total sample.

Using the results presented in Tables (4-4)&(4-5)&(4-6)&(4-8) and (4-9) which represent the results obtained from laboratory of the Libyan Iron and Steel Company in Misurata in equation (5-1) with the dielectric constant of each substance as given in [1], and using program (1) in Appendix (B) , the dielectric constant of each sample is given in Tables (5-1a,b) , (5-2a,b) , (5-3a,b) , (5-4) , (5-5a,b) , (5-6) and (5-7) respectively .

Table (5-1a) From LISCO Analysis of Sample No. 1

Compound	$\epsilon' + j\epsilon''$	V	$\epsilon^{1/3} V$
SiO_2	4.43-j0.04	0.9030	1.481-j0.0045
Al_2O_3	12.66-j1.31	0.0415	0.0968-j0.0033
Fe_2O_3	16.58-j0.93	0.00363	0.0093-j0.0002
$CaCO_3$	5.01-j0.08	0.0168	0.0287-j0.0002
$MgCO_3$	5.03-j0.17	0.00752	0.0129-j0.0001

From the last column in Table (5-1a) and equation (5-1) the complex dielectric constant of the mixture is. ϵ_r = **4.3367-j0.0659**

In the previous table we ignored (KCl, NaCl , SO_3 ,TiO_2 ,P_2O_5) due to the lack of information about their dielectric constants (the volume of the ignored items totals to 0.0275 out of normalized volume of one). Having we normalized Table (5-1a) by considering the sample made up of only five items we get the results presented in Table (5-1b) .

Table (5-1b) Results of (5-1a) after normalization

Compound	$\epsilon' + j\epsilon''$	V	$\epsilon^{1/3} V$
SiO_2	4.43-j0.04	0.9285	1.5228-j.004627
Al_2O_3	12.66-j1.31	0.04267	0.09953-j.00339
Fe_2O_3	16.58-j0.93	0.00373	0.0096-j0.00021
$CaCO_3$	5.01-j0.08	0.0172	0.0294-j0.00021
$MgCO_3$	5.03-j0.17	0.007733	0.0133-j0.0001

From the last column in Table (5-1b) and equation (5-1) the complex dielectric constant of the mixture is . ϵ_r = **4.6959-j0.0718**

The two results give percentage error in the real part is 7.649% , and the percentage error in the imaginary part is 8.2% .

Table (5-2a) From LISCO Analysis of Sample No. 2

Compound	$\epsilon' + j\epsilon''$	V	$\epsilon^{1/3} V$
SiO_2	4.43-j0.04	0.8799	1.4451-j0.0043
Al_2O_3	12.66-j1.31	0.0485	0.1132-j0.0039
Fe_2O_3	16.58-j0.93	0.00708	0.0181-j0.0003
$CaCO_3$	5.01-j0.08	0.0350	0.0599-j0.0003
$MgCO_3$	5.03-j0.17	0.00709	0.0121-j0.0001

From the last column in Table (5-2a) and equation (5-1) the complex dielectric constant of the mixture is . ϵ_r=**4.3328- j0.071**

In the previous table we again ignored (KCl, NaCl ,TiO_2 ,P_2O_5 ZrO_2 , MnO) due to the lack of information about their dielectric constants ,(the volume of the ignored items totals to 0.0224 out of the normalized volume of one). Have we normalized Table (5-2a) by considering the sample made up of only five items we get the following table.

Table (5-2b) Results of (5-2a) after Normalization

Compound	$\epsilon' + j\epsilon''$	V	$\epsilon^{1/3} V$
SiO_2	4.43-j0.04	0.90006	1.4782-j0.0044
Al_2O_3	12.66-j1.31	0.0496	0.1158-j0.00307
Fe_2O_3	16.58-j0.93	0.007242	0.0185-j0.0003
$CaCO_3$	5.01-j0.08	0.03580	0.061-j0.00031
$MgCO_3$	5.03-j0.17	0.0072525	0.0124-j0.0001

From the last column in Table (5-2a) and equation (5-1) the complex dielectric constant of the mixture is . ϵ_r **= 4.7914 - j0.0697**

The percentage error in the real part is 9.6% , and the percentage error in the imaginary part is 1.87%

Table (5-3a) From LISCO Analysis of Sample No. 3

Compound	$\epsilon' + j\epsilon''$	V	$\epsilon^{1/3} V$
SiO_2	4.43-j0.04	0.3893	0.6394-j0.0019
Al_2O_3	12.66-j1.31	0.0607	0.1416-j0.0049
Fe_2O_3	16.58-j0.93	0.0129	0.0329-j0.0006
$CaCO_3$	5.01-j0.08	0.4954	0.8477-j0.0045
$MgCO_3$	5.03-j0.17	0.0146	0.0250-j0.0003

From the last column in Table (5-3a) and equation (5-1) the complex dielectric constant of the mixture is . ϵ_r **=4.7974- j0.1041**

In the previous table we again ignored (KCl, NaCl) due to the lack of information about their dielectric constants ,the volume of the ignored items totals to 0.0271 . Have we normalized table (5-3a) by considering the sample made up of only five items we get the following table.

Table (5-3b) Results of (5-3a) after Normalization

Compound	$\epsilon' + j\epsilon''$	V	$\epsilon^{1/3} V$
SiO_2	4.43-j0.04	0.4001	0.6572-j0.0020
Al_2O_3	12.66-j1.31	0.0624	0.1456-j0.0050
Fe_2O_3	16.58-j0.93	0.0133	0.0338-j0.0006
$CaCO_3$	5.01-j0.08	0.5092	0.8713-j0.0046
$MgCO_3$	5.03-j0.17	0.0150	0.0257-j0.0003

From the last column in Table (5-3b) and equation (5-1) the complex dielectric constant of the mixture is . ϵ_r = **5.2093-j0.1127**

The percentage error in the real part is 7.9%, and the percentage error in the imaginary part is 7.63% . This error can be considered small.

Table (5-4) From LISCO Analysis of Sample No. 4

Compound	$\epsilon' + j\epsilon''$	V	$\epsilon^{1/3} V$
SiO_2	4.43-j0.04	0.6691	1.0989-j0.0033
CaCO3	5.03-j0.17	0.2240	0.3833-j0.0020
$MgCO_3$	16.58-j0.93	0.0108	0.0185-j0.0002
Fe_2O_3	5.01-j0.08	0.0443	0.1130-j0.0021
Al_2O_3	12.66-j1.31	0.0215	0.0502-j0.0017

From the last column in Table (5-4) and equation (5-1) the complex dielectric constant of the mixture is . ϵ_r = **4.6062-j0.078**

With the laboratory results we received a note that the previous sample contained high carbon with major part of it, got burned during the analysis, this could explain the big drop in the volume of the five main constituents.

Table (5-5a) From LISCO Analysis of Sample No. 5

Compound	$\epsilon' + j\epsilon''$	V	$\epsilon^{1/3} V$
SiO_2	4.43-j0.04	0.3148	0.5170-j0.0016
$CaCO_3$	5.01-j0.08	0.4886	0.8361-j0.0044
$MgCO_3$	5.03-j0.17	0.0163	0.0279-j0.0003
Fe_2O_3	16.58-j0.93	0.0420	0.1071-j0.0020
Al_2O_3	12.66-j1.31	0.0168	0.0392-j0.0013

From the last column in Table (5-5a) and equation (5-1) the complex dielectric constant of the mixture is . ϵ_r =**3.5626-j0.0677**

The volume of the ignored components of the sample totals to 0.1215 which has a percentage of 13.83 % .Again if we consider the sample to be made of only the five items

Table (5-5b) Results of (5-5a) after Normalization

Compound	$\epsilon' + j\epsilon''$	V	$\epsilon^{1/3} V$
SiO_2	4.43-j0.04	0.3583	0.5885-j0.0018
$CaCO_3$	5.03-j0.17	0.5561	0.9516-.j0.0051
$MgCO_3$	16.58-j0.93	0.0185	0.0317-j0.0004
Fe_2O_3	5.01-j0.08	0.0478	0.1219-g0.0023
Al_2O_3	12.66-j1.31	0.0191	0.0446-j0.0015

From the last column in Table (5-5b) and equation (5-1) the complex dielectric constant of the mixture is . ϵ_r =**5.252-j0.1006**

This gives an error of 32.166% in the real part and 32.703% in the imaginary part. The average of the two approaches is 4.4073-j0.08415

Table (5-6) From LISCO Analysis of Sample No. 6

Compound	$\epsilon' + j\epsilon''$	V	$\epsilon^{1/3} V$
SiO_2	4.43-j0.04	0.5807	0.9537-j0.0029
$CaCO_3$	5.01-j0.08	0.3368	0.5763-j0.0031
$MgCO_3$	5.03-j0.17	0.0118	0.0202-j0.0002
Fe_2O_3	16.58-j0.93	0.0402	0.1025-j0.0019
Al_2O_3	12.66-j1.31	0.0100	0.0233-j0.0008

From the last column in Table (5-6) and equation (5-1) the complex dielectric constant of the mixture is . ϵ_r = **4.7074-j0.0750**

Table (5-7) From LISCO Analysis of Sample No. 10

Compound	$\epsilon' + j\epsilon''$	V	$\epsilon^{1/3} V$
SiO_2	4.43-j0.04	0.9110	1.4962-j0.0045
$CaCO_3$	5.01-j0.08	0.0417	0.0714-j0.0004
$MgCO_3$	5.03-j0.17	0.0020	0.0034-j0.0000
Fe_2O_3	16.58-j0.93	0.0310	0.0791-j0.0015
Al_2O_3	12.66-j1.31	0.0150	0.0350-j0.0012

From the last column in Table (5-7) and equation (5-1) the complex dielectric constant of the mixture is , $\mathbf{\epsilon_r = 4.7847 - j0.0647}$

The value of dielectric constant of all samples for results in Libyan Iron and Steel Company from Tables (5-1a), (5-2a), (5-3a), (5-4) , (5-5a), (5-6), (5-7), as given by :

Table (5-8) Results from LISCO

Sample No.	Type	ϵ_m
1	Sand	4.3367-j0.0659
2	Sand	4.3328-j0.0710
3	Sand	4.7974-j0.1041
4	Sand	4.6062-j0.0780
5	Dust	3.5626-j0.0677
6	Sand	4.7074-j0.0750
10	Sand	4.7847-j0.0647

The normalized value of dielectric constant from Tables (5-1b), (5-2b), (5-3b), (5-5b), as given in Table (5-9):

Table (5-9) Results when the sample is normalized

Sample No.	Type	ϵ_m
1	Sand	4.6959-j0.0718
2	Sand	4.7914-j0.0697
3	Sand	5.2093-j0.1127
5	Dust	5.252-j0.1006

Analysis of samples obtained from the Libyan Petroleum Institute gave the constituents not in compound form i.e. not as oxides but as separate elements, this does not reflect the actual components so we will not use it to find the attenuation constant and their results will be used to find the PSD .

From the pervious tables the following remarks, can be pointed out

- The percentage of silicon oxide in the samples increases as we move south (far from the sea side)
- The percentage of Aluminum oxide in the samples increases as we move north (towards the sea side)
- The percentage of Ferro-oxide in the samples reaches it's heights value at the mid section and decreases in both directions of it.
- The average of dielectric constant from Table (5-8) equal to 4.4468-j0.0752.
- The average of dielectric constant from Table (5-9) equal to 4.9871-j0.0887.
- The average of the dielectric constant from the two approaches is

  ϵ_r =4.71965-j0.08195 and this could be used as the effective dielectric constant for the studied area of Libya.

5-3 Calculation of the probability from PSD analysis:

From the results presented in Tables (4-11) to (4-15).The distribution probability can be obtained as given in the following tables (5-10a) to (5-10e) respectively

Table (5-10a) PSD for Sample (2) from the Libyan Petroleum Institute

Particle Diameter (μm)	Probability
850-600	0.105811
425-355	0.2677522
300-212	0.3255428
180-150	0.1218391
125-90	0.1305875
75-25	0.04763729

Table (5-10b) PSD for Sample (9) from the Libyan Petroleum Institute

Particle Diameter (μm)	Probability
850-600	0.0000
425-355	0.00655172
300-212	0.1089655
180-150	0.1512069
125-90	0.5072414
75-25	0.1998276

Table (5-10c) PSD for Sample (8) from the Libyan Petroleum Institute

Particle Diameter (μm)	Probability
850-600	0.01222559
425-355	0.1769871
300-212	0.5850492
180-150	0.1588191
125-90	0.06222559
75-25	0.00598032

Table (5-10d) PSD for Sample (6) from the Libyan Petroleum Institute

Particle Diameter (μm)	Probability
850-600	0.1573402
425-355	0.1786701
300-212	0.2840668
180-150	0.1390941
125-90	0.05255381
75-25	0.1810793

Table (5-10e) PSD for Sample (5) from the Libyan Petroleum Institute

Particle Diameter (μm)	Probability
850-600	0.0000
425-355	0.0541045
300-212	0.02276119
180-150	0.04682836
125-90	0.3764925
75-25	0.548694

The results of Tables (4-7), (4-8) , (5-10a to 5-10e) are plotted in Figures (5-1a) and (5-1b) . The plotting are generated by a computer programs (2) and (3) in appendix (B).

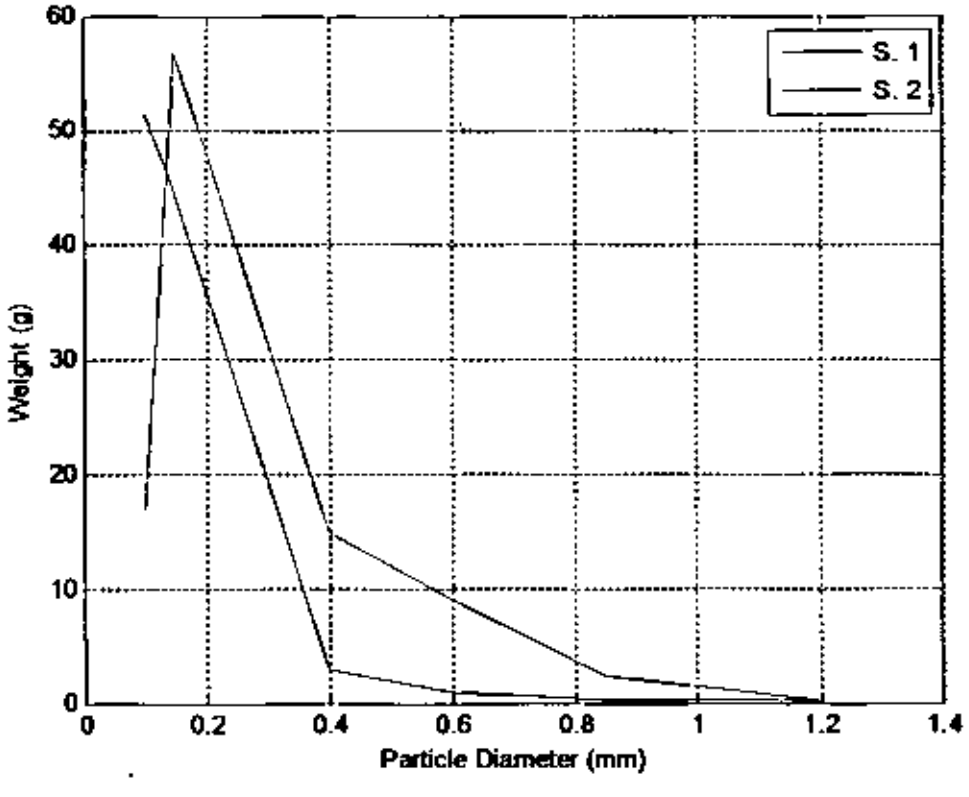

Fig. (5.1a) PSD Curves from Libyan Iron and Steel Company

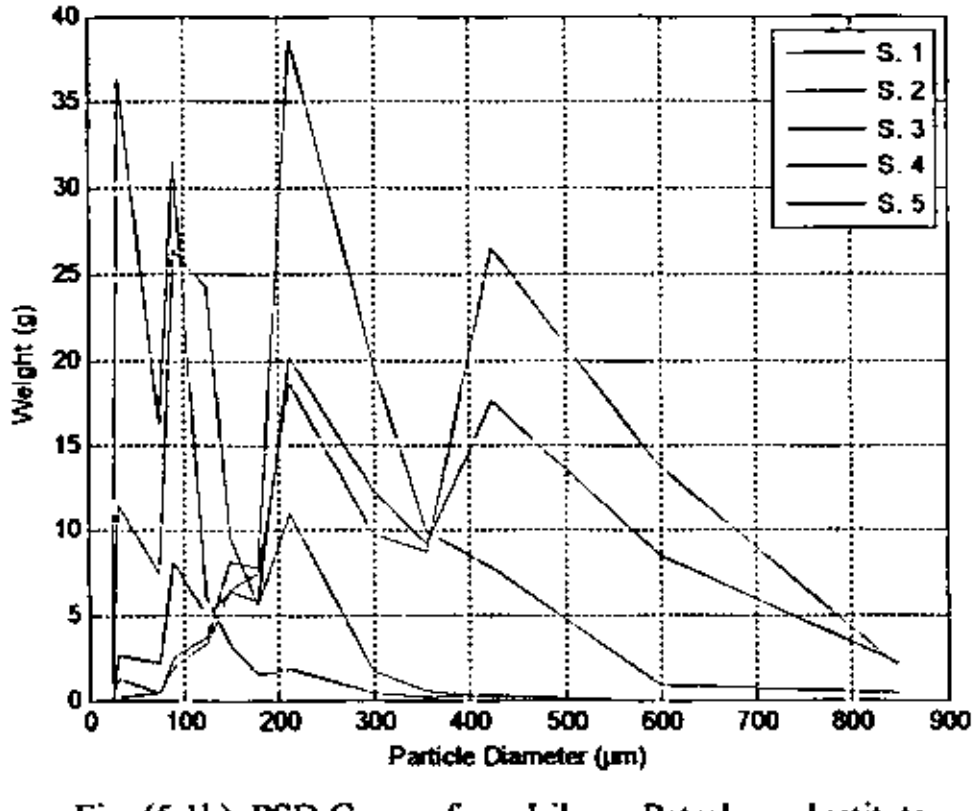

Fig. (5.1b) PSD Curves from Libyan Petroleum Institute

- From Tables (4-7) and (4-8) the biggest quantity (percentage) has a radius of 150 micro meter
- For the five samples presented in Tables (4-11) to (4-15) the highest quantity (percentage) for sand samples has radius of 212 micro meter while that for the dust samples was 90 micrometer.
- So based on that the sample can be classified as sand if it has radius 150 micrometer and higher. If the PSD is lower than 150 micrometer it is named as dust.

5.4 Estimating the visibility from meteorological data:

Meteorological data recorded for Libya lacks any information about the visibility, so we decided to estimate it by considering it inversely proportional to the wind speed, to find the constant of proportionality we depended on the visibility value that we personally measured during the storm that happened on 24-02-2006 which we measured it as 100 m at speed of 30 knots.

$$\text{Visibility} = \frac{\text{Constant}}{\text{Speed}} \quad \text{----------} \quad (5\text{-}2)$$

$$V = \frac{K}{S} \quad \text{----------} \quad (5\text{-}3)$$

$$100 = \frac{K}{30} \quad \text{----------} \quad (5\text{-}4)$$

$$K = 3000$$

$$V_i = \frac{3000}{S_i} \quad \text{----------} \quad (5\text{-}5)$$

Where:

V_i is the visibility in meters,

S_i is the wind speed in knots.

Using the data provided to us by the metrological center in Tripoli for the wind speed data for fourteen years we were able to estimate the visibility for the sites of concern for the months that has the highest wind.

Table (5-11a) The Visibility in Agedabia

Year	DEC.		JAN.		FEB.		MAR.		APR.		MAY.	
	S	V	S	V	S	V	S	V	S	V	S	V
1990	29	103.4	27	111.1	20	150	20	150	20	150	20	150
1991	24	125	21	142.8	22	136.3	32	93.7	24	125	27	111.1
1992	20	150	15	200	20	150	34	88.2	23	130.4	35	85.7
1993	16	187.5	13	230.7	17	176.4	22	136.3	18	166.6	18	166.6
1994	20	150	23	130.4	20	150	18	166.6	25	120	22	136.3
1995	15	200	23	130.4	15	200	20	150	22	136.3	20	150
1996	25	120	27	111.1	25	120	26	115.3	38	78.9	25	120
1997	38	78.9	28	107.1	30	100	26	115.3	30	100	30	100
1998	25	120	20	150	20	150	26	115.3	27	111.1	25	120
1999	22	136.3	20	150	23	130.4	30	100	28	107.1	20	150
2000	18	166.6	20	150	20	150	25	120	38	78.9	25	120
2001	22	136.3	25	120	30	100	20	150	23	130.4	30	100
2002	18	166.6	20	150	28	107.1	28	107.1	35	85.7	26	115.3
2003	25	120	20	150	27	111.1	30	100	25	120	25	120

Table (5-11b) The Visibility in Jalo

Year	DEC.		JAN.		FEB.		MAR.		APR.		MAY.	
	S	V	S	V	S	V	S	V	S	V	S	V
1990	19	157.8	21	142.8	16	187.5	17	176.4	25	120	20	150
1991	23	130.4	18	166.6	22	136.3	25	120	24	125	25	120
1992	20	150	16	187.5	20	150	30	100	28	107.1	19	157.8
1993	18	166.6	12	250	20	150	23	130.4	18	166.6	29	103.4
1994	15	200	30	100	20	150	22	136.3	29	103.4	42	71.4
1995	18	166.6	15	200	20	150	30	100	21	142.8	20	150
1996	20	150	20	150	38	78.9	20	150	30	100	20	150
1997	24	125	18	166.6	25	120	30	100	33	90.9	18	166.6
1998	20	150	18	166.6	18	166.6	30	100	20	150	25	120
1999	20	150	20	150	25	120	20	150	27	111.1	25	120
2000	20	150	18	166.6	20	150	25	120	35	85.7	35	85.7
2001	30	100	25	120	25	120	28	107.1	27	111.1	32	93.7
2002	20	150	22	136.3	24	125	27	111.1	25	120	27	111.1
2003	18	166.6	20	150	32	93.7	26	115.3	30	100	26	115.3

The visibility for the six months during which the storms peak can be calculated using the data presented in Tables (4-1) and (4-2), and using program (4) in Appendix (B), the visibility for these months are shown in Tables (5-11a) and (5-11b) respectively from which we see that the lowest visibility was around 71.4 meter and it occurred on May 1994 , instead of using the visibility on a monthly basis we believe that working with the average visibility over the six months period along with the average speed is much better. This is as if we were using a fitting to the data before using it, the average speed along with the average visibility is given in Table (5-12) with this approach the minimum average visibility in Jalo was 108.65 meter and the minimum average visibility in Agedabia was 100.21 meter

Table (5-12) Average of Visibility in Jalo and Agedabia

Year	Jalo		Agedabia	
	Average		Average	
	S(k.)	V(m)	S(k.)	V(m)
1990	19.6	155.75	22.6	135.75
1991	22.8	133.05	25	122.31
1992	22.1	142.06	24.5	134.05
1993	20	161.16	17.3	177.35
1994	26.3	126.85	21.3	142.21
1995	20.6	151.56	19.1	161.11
1996	24.6	129.81	27.6	110.88
1997	24.6	128.18	30.3	100.21
1998	21.8	142.2	23.8	127.73
1999	22.8	133.51	23.8	126.96
2000	25.5	126.33	24.3	130.91
2001	27.8	108.65	25	122.78
2002	24.1	125.58	25.8	121.96
2003	25.3	123.48	25.3	120.18

5-5 Estimating the Wave Attenuation :

For dust, the imaginary part of the dielectric constant is very dependent on the hygroscopic water content of the sample this can be concluded from the variations of the dielectric constant with humidity of the sample. Attenuation depends on the shape of the scattering particles and their orientation relative to the wave polarization, and the attenuation due to scattering is small and may be neglected and this is based on our finding of small radius of the suspended particles. Microscopic investigation revealed that the average axes ratios for the best fit ellipsoid are 1: 0.75: (0.75).[5] with the biggest dimensions as the PSD.

In this study, two methods for calculating the attenuation are used:

5-5-1 Method (1):-

The optical visibility V (in kilometers) and the optical attenuation per kilometer α, are related by the simple relation [3]

$$V = 15/\alpha \qquad \text{..... (5-6)}$$

For spherical particles of effective radius a_e (meters), and the complex relative permittivity of the particles ($\epsilon = \varepsilon' + j\varepsilon''$), the attenuation coefficient (α) can be found from [3]:

$$\alpha = \frac{189}{V}\frac{a_e}{\lambda}\frac{3\varepsilon''}{(\varepsilon' + 2)^2 + \varepsilon''^2} \qquad \text{..... (5-7)}$$

Where λ is the wavelength (in meters)

From average values of dielectric constant given in Tables (5-8) and (5-9) and the average visibility from table (5-12) , at a frequency of 3Ghz with the effective radius equals 0.000075 m from the PSD data, the attenuation coefficient can be calculate using equation (5-7), and using program (5) in Appendix (B) ,with the results given in Table (5-13), and

drawn in Fig .(5.2). This table gives an average attenuation of 0.00566 (dB/km) which is too small to effect over the microwave link under consideration even for the longest hop distance . .

Table (5-13)The Value of Attenuation Using Method (1)

Visibility(km)	Attenuation(dB/km)
0.10021	0.0071
0.10865	0.0066
0.11088	0.0064
0.12018	0.0059
0.12231	0.0058
0.12348	0.0058
0.12773	0.0056
0.14221	0.0050
0.16111	0.0044
0.17735	0.0040

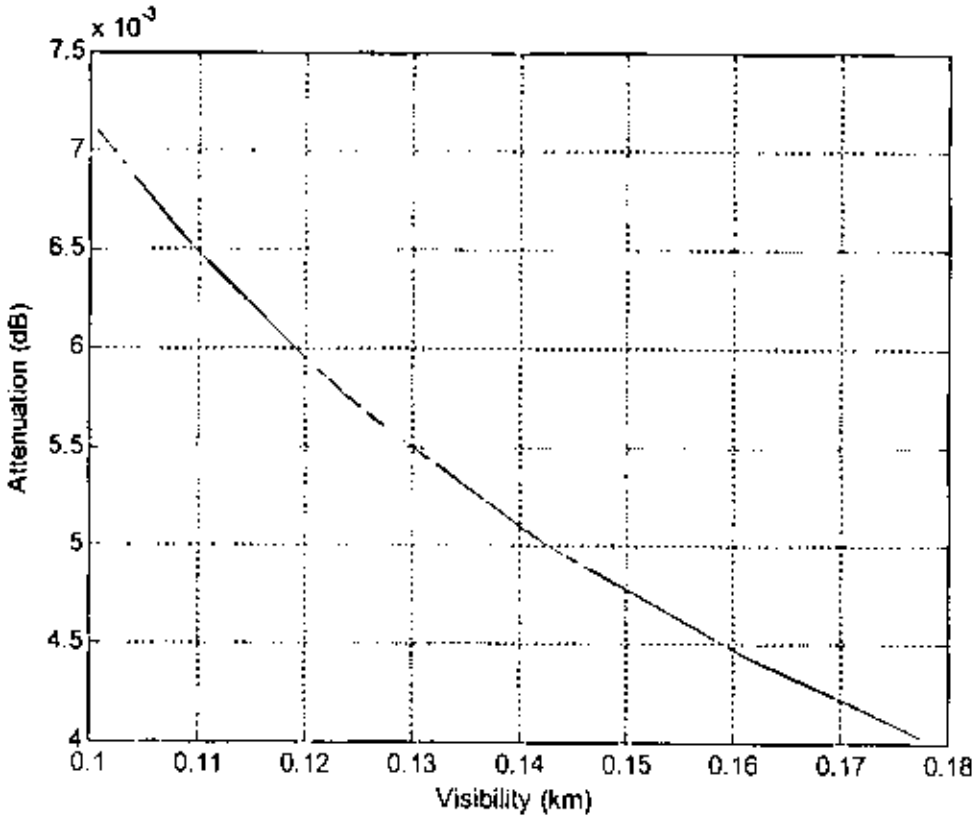

Fig. (5.2) The Relation Between Attenuation and Visibility

5.5.2 Method (2) :-

In this section we will use exactly the same expression obtained by Ghobrial [1] using an analysis based on the work of Maxwell Garnett. Equation (5-8) used to determine the attenuation when a wave of known polarization propagates through a storm.

$$\alpha = \frac{2.46 v \varepsilon'' \times 10^5}{[(\varepsilon' + 2)^2 + \varepsilon''^2]\lambda} \quad \text{dB/km} \quad \ldots\ldots\ldots\ldots\ldots\ldots (5\text{-}8)$$

When v is the relative volume occupied by dust particles in a storm is obtained from

$$v = \frac{C}{\rho V^{\gamma}} \quad \text{m}^3/\text{m}^3 \ldots\ldots\ldots\ldots\ldots\ldots\ldots\ldots\ldots\ldots\ldots\ldots\ldots\ldots\ldots\ldots (5\text{-}9)$$

Where C and γ are constants that depend on the distance from the point of origin of the storm, type of soil and climatic conditions at the origin. The following values are believed to be applicable to conditions in Sudan and the same in Libya:

$$C = 2.3 \times 10^{-5} \ , \ \gamma = 1.07.$$

The average measured density of the six samples collected in Libya from Table (4-9) is 1.5067 gm/cm^3.

Then :

$$v = \frac{1.5265 \times 10^{-8}}{V^{1.07}} \quad \text{m}^3/\text{m}^3 \ldots\ldots\ldots\ldots\ldots\ldots\ldots\ldots\ldots\ldots\ldots\ldots\ldots\ldots\ldots\ldots (5\text{-}10)$$

The attenuation of the circularly polarized wave is brought about by two mechanisms,

- Absorption of energy in the propagation medium.
- Change in polarization.

All of the parameters of equation (5-8) are defined in the previous section application of which results in the attenuation values as presented in Table (5-14) and Figure (4.3) by using program (6) in Appendix (B) The average of the attenuation is 0.00628 db/km. This is almost as that found using method (1) (0.00566 db/km)

Table (5-14) The Value of Attenuation Method (2)

Visibility(km)	Attenuation(dB/km)
0.10021	0.0080
0.10865	0.0073
0.11088	0.0072
0.12018	0.0066
0.12231	0.0065
0.12348	0.0064
0.12773	0.0062
0.14221	0.0055
0.16111	0.0048
0.17735	0.0043

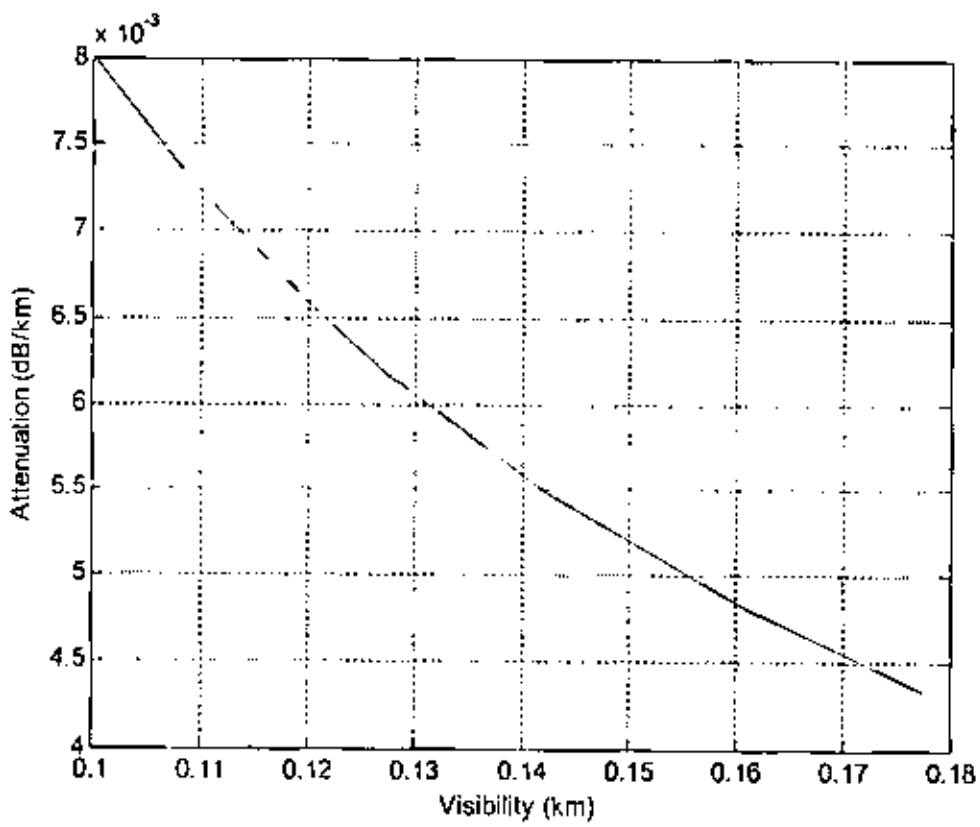

Fig. (5.3) The Relation Between Attenuation and Visibility

CHAPTER 6

Conclusions and Recommendations

6-1 Conclusions:

From the samples that we collected using the standard approach used by panniers and analyzed in the best two laboratories in the country one can draw the following remarks:

- The two laboratories give close results for some samples while they give differing results for some others when they use different approach.
- From the sand sample results we found that the percentage of silicon oxide in the sample increases as one moves south.
- The main metals in samples are Aluminum oxide and ferrite oxide they have percentage that average to about 7 %. One can notice that : Ferrite oxide has it's highest percentage at the middle region of area studied and it decreases s as one moves in both directions of it, Aluminum oxide has it's lowest percentage at the middle region of area studied and it increases as one moves in both directions of it.
- The studied area has wind storms that peaks during the months from Dec. through May with the fastest recorded storm in Jalo with a speed of 42 knots and lowered the visibility to 71.4 meters.
- The average relative dielectric constant for the selected area of Libya found to be $\epsilon_r = 4.71965 - j0.08195$ and this results in an attenuation coefficient which averaged to 0.00597db/km , while that for the north of Sudan is 0.0097db/km [2], the difference is expected due to the difference in the constituents.

- The attenuation to signal of the Great man made river that results from the dust and storms is negligible, this is based on the average attenuation per unit length and the maximum distance between stations which is 55 km (total attenuation 0.328 dB).

- Based on the PSD analysis we classified the samples as dust if the diameter is equal to or less than 150 micro meters and the samples can be considered as sand if the diameter is greater than 150 micro meters.

- The value of the dielectric constant found is at a frequency of 3 GHz we expect the attenuation to increases as the frequency increases this is because as the frequency increase the wavelength decreases results in an increase of the electrical dimension of the suspended particles

6-2 Recommendations:

- In this study we did not study the scattering effect because we were unable to find the exact dimensions of the particles, so a continuation to this work could be executed to study scattering.

- An experimental study should be conducted by designing ,and building a special microwave link that monitor the effect of storms over a couple of years

- The results of this study should not be drawn for all of Libya , but it is valid for the studied area and any similar part only , for other parts that is not similar like Sabha (Wadi Shatty) were ferrite and other metals exits with high percentage a parallel study should be conducted.

References:

1- *S. I. Ghobrial and S. M. Sharief*, "Microwave attenuation and cross polarization in dust storms," *IEEE Trans. Antennas Propagat.*, vol. AP-35, pp. 418–425, Apr. 1987.

2- "Attenuation and Backscatter From a Derived Two-Dimensional Dust storm Model "***Julius Goldhirsh, Life Fellow, IEEE,2001.***

3- *A.A. Ali* "Optimum hop length for millimetre wave radio links in an arid climate "", IEE, 1995.

4- ***Shakir, A.A.***; H.M. AL-Rizzo and M.M. Cyril ;" Practical –Size Distribution of Iraq sand and dust storm and their Influence on Microwave communication systems"; IEEE Tran Antenna and propagation vol 36 no 1 Jan 1988 pp 114-126.

5- Terrestrial Digital Microwave Communications; ***Ferdo Ivanek***, editor .Artech House ,1989 .

6- Microwave Transmission for Telecommunication ; ***Paul F. Combes*** ,1991 .

7- Design Handbook for Line of Sight Microwave Communication System, 1977.

8- Meteorological data from the weather watch in Tripoli- Libya.

9- ***Sami Sharif*** "Chemical and Mineral Composition of Dust and Its Effect on The Dielectric Constant", *IEEE Trans.*, vol. 33, NO. 2, March. 1995.

10- ***S.M. ELhabashi and Hassan ALdeeb*** " Chemical composition of dust and sand in Libya" accepted for publication in Investment in technology conference Mina University, Egypt 7-8 May 2007.

Appendix (A)

MAXIMUM WIND SPEED Knots — العنصر : اقصى سرعة للرياح بالعقدة

STATION NAME & NO. : AGEDABIA 62055 — اسم المحطة : اجدابيا

PERIOD : (1956-2003) LAT. 30 43 N LON. 20 10 E ELV. 07 M — الفترة : (2003-1956)

YEAR	JAN	FEB.	MAR.	APR.	MAY	JUN	JUL	AUG.	SEP.	OCT.	NOV.	DEC.
1990	120/27	330/20	180/20	330/20	090/20	170/20	350/20	330/19	350/20	090/18	060/23	300/29
1991	300/21	090/22	090/32	330/24	180/27	340/19	310/20	350/20	330/15	340/21	030/18	330/24
1992	090/15	330/20	110/34	160/23	090/35	100/18	330/20	330/22	330/20	160/19	330/14	160/20
1993	270/13	060/17	300/22	330/18	110/18	300/18	300/22	340/18	160/20	170/20	120/18	330/16
1994	330/23	170/20	350/18	140/25	360/22	330/17	330/20	330/22	330/18	200/23	200/15	300/20
1995	270/23	330/15	180/20	220/22	180/20	110/18	350/19	330/21	360/20	360/18	120/18	270/15
1996	140/27	270/25	330/26	350/38	180/25	070/23	330/22	360/20	160/20	160/20	330/20	320/25
1997	330/28	360/30	180/26	300/30	090/30	360/23	360/24	330/23	330/22	180/25	160/20	310/38
1998	300/20	020/20	120/26	180/27	330/25	360/20	360/21	360/18	330/22	360/22	300/20	180/25
1999	120/20	120/23	180/30	160/28	330/20	350/20	360/20	360/20	360/20	360/18	090/25	330/22
2000	160/20	350/20	360/25	360/38	180/25	350/28	360/22	360/22	180/20	160/20	360/26	360/18
2001	180/25	310/30	360/20	270/23	350/30	350/20	360/23	360/20	180/20	360/18	180/20	270/22
2002	360/20	360/28	360/28	240/35	180/26	350/23	360/25	360/25	090/23	240/18	320/22	300/18
2003	360/20	360/27	180/30	180/25	350/25	150/22	030/20	360/20	360/22	360/14	320/20	180/25

MAXIMUM WIND SPEED Knots — الحصر : اقصى سرعة للرياح بالعقدة

STATION NAME & NO. : JALO 62161 — اسم المحطة : جالو

PERIOD (1956-2003) LAT. 29-02 N LON. 21-34 E ELV. 60 M — الفترة : (2003-1956)

YEAR	JAN	FEB	MAR	APR	MAY	JUN	JUL.	AUG	SEP.	OCT.	NOV.	DEC
1990	300/21	270/16	360/17	290/25	330/20	160/19	360/15	330/14	260/15	200/19	140/25	280/19
1991	290/18	300/22	120/25	180/24	320/25	350/12	340/12	360/12	190/15	360/18	140/15	280/23
1992	280/16	280/20	280/30	180/28	310/19	140/18	350/11	340/11	330/14	160/13	310/22	170/20
1993	290/12	280/20	320/23	360/18	220/29	330/15	340/16	320/13	190/17	120/10	170/15	270/18
1994	270/30	290/20	330/22	120/29	300/42	330/16	330/12	330/15	330/10	340/12	070/15	260/15
1995	220/15	340/20	170/30	270/21	240/20	330/17	340/20	180/15	170/20	180/20	190/18	180/18
1996	190/20	270/38	350/20	180/30	120/20	360/18	340/20	360/20	180/20	330/18	190/19	270/20
1997	320/18	350/25	360/30	340/33	330/18	350/20	340/24	270/20	360/20	350/25	180/25	280/24
1998	220/18	290/18	190/30	170/20	350/25	350/20	350/20	360/16	200/17	190/20	170/20	360/20
1999	290/20	270/25	170/20	170/27	320/25	350/19	360/20	350/15	350/20	360/20	170/20	330/20
2000	340/18	210/20	270/25	330/35	150/35	350/22	350/20	360/20	170/23	180/20	330/18	180/20
2001	270/25	330/25	180/28	180/27	330/32	350/15	360/20	190/20	240/19	350/18	300/25	270/30
2002	210/22	300/24	300/27	160/25	360/27	350/28	330/25	360/18	180/20	300/18	170/20	240/20
2003	200/20	300/32	260/26	150/30	330/26	350/20	360/20	350/16	100/20	350/14	360/20	210/15

ARL-XRF/UniQuant Analysis Report

QUALITY CONTROL DEPARTMENT TS.19
TESTS & ANALYSIS SECTION

C:\XRF\UQ4\JOB\JOB.515
Sample ident = Sand - 01

Oxide	Mass%	StdErr	El	Mass%	StdErr
SiO2	90.30	0.30	Si	42.22	0.14
Al2O3	4.15	0.10	Al	2.20	0.05
CaCO3	1.68	0.13	Ca	1.20	0.09
KCl	1.62	0.10	K	0.850	0.052
NaCl	1.150	0.083	Na	0.580	0.062
MgCO3	0.752	0.037	Mg	0.453	0.022
SO3	0.489	0.022	Sx	0.196	0.009
Fe2O3	0.363	0.049	Fe	0.254	0.035
TiO2	0.0835	0.0067	Ti	0.0501	0.0040
P2O5	0.0711	0.0058	Px	0.0310	0.0025

Known: Diluent/Sample = 0.500 Diluent = B2O3

ARL-XRF/UniQuant Analysis Report

QUALITY CONTROL DEPARTMENT TS.19
TESTS & ANALYSIS SECTION

C:\XRF\UQ4\JOB\JOB.516
Sample ident = Sand - 02

Oxide	Mass%	StdErr	El	Mass%	StdErr
SiO2	87.99	0.32	Si	41.14	0.15
Al2O3	4.85	0.10	Al	2.57	0.06
CaCO3	3.50	0.20	Ca	2.50	0.14
KCl	1.818	0.11	K	0.952	0.057
MgCO3	0.709	0.035	Mg	0.428	0.021
Fe2O3	0.708	0.078	Fe	0.495	0.055
NaCl	0.864	0.058	Na	0.340	0.043
TiO2	0.241	0.016	Ti	0.145	0.010
ZrO2	0.221	0.034	Zr	0.164	0.025
P2O5	0.0711	0.0058	Px	0.0310	0.0025
MnO	0.0203	0.0018	Mn	0.0157	0.0014
SO3	0.0133	0.0028	Sx	0.0053	0.0011

Known: Diluent/Sample = 0.500 Diluent = B2O3

التركيب الكيميائي والتوزيع الحجمي لعينات رمل

Fe_2O_3	$NaCl$	KCl	$MgCO_3$	$CaCO_3$	Al_2O_3	SiO_2	رقم العينة
0.454	2.15	2.12	1.07	2.83	6.89	84.69	3

المجموع	< 0.15	$0.15mm$	$0.40mm$	$0.60mm$	$0.85mm$	$1.2mm$	رقم العينة
1004.90	515.30g	446.50g	28.20g	10.60g	2.30g	2.00g	3
100.00	51.28	44.43	2.81	1.05	0.23	0.20	%

Fe_2O_3	$NaCl$	KCl	$MgCO_3$	$CaCO_3$	Al_2O_3	SiO_2	رقم العينة
1.29	1.02	1.43	1.46	49.54	6.07	38.93	4

المجموع	< 0.15	$0.15mm$	$0.40mm$	$0.60mm$	$0.85mm$	$1.2mm$	رقم العينة
1064.70	180.00g	604.80g	157.90g	95.50g	24.60g	1.90g	4
100.00	16.91	56.80	14.83	8.97	2.31	0.18	%

رقم العينة	فاقد الحرق	SiO_2	CaO	MgO	Fe_2O_3	Al_2O_3
4	32.24%	66.91	22.40	1.08	4.43	2.15
5	18.10%	31.48	48.86	1.63	4.20	1.68
6	22.67%	58.07	33.68	1.18	4.02	1.00
10	1.72%	91.10	4.17	0.20	3.10	1.50

Conductivity (ms)	Density (g/cm^3)	رقم العينة
240	1.49	2
797	1.53	5
6.54	1.11	6
1660	1.62	7
90	1.72	8
565	1.57	9

TEST REPORT

Issued by : Libyan Petroleum Institute

Date of Issue : 11/07/2006

Test Report No : 0012/IL20/06

Customer	: جامعة البحدي
Address	: جامعة البحدي سرت
Date sample received	: 06/06/2006
Sample identification	: Sand
Work order No	: 0179/IL20/06
Sample condition upon receiving	: Physically is in good condition
Testing date	: 2/07/2006
Customer requested date	: N/A
Testing venue	: IL20 (Analytical Chemistry
Temperature	: N/A
Relative Humidity	: N/A
Sampling procedure used	: Done by Client
Sampling date	: N/A
Test Method	: ASTM method
Testing outcome	: Compliance with the requirement
Measurement uncertainty	: N/A
Opinion and interpretations	:N/A

info@nilibya.org

Issued by : Libyan Petroleum Institute
Date of Issue : 11/07/2006

Test Report No : 0012/IL20/06

Table 1:-

Sample No.	SiO_2 (%)	Ca^{++} (%)	Mg^{++} (%)	Na^{+}(ppm)	K^{+}(ppm)	Cl^{-} (ppm)	Conductivity (µmhos/cm)
1	95.373	1.042	0.0926	37	4.5	92	169(23.4)
2	83.673	3.820	0.206	31	6	63	195.1(23.3)
3	90.525	3.047	0.158	7	2.5	23	24.3(23.2)
4	57.067	2.815	1.913	3.5	1	16	33.3(23.2)
5	5.280	3.060	1.991	55	10	101	260(23.0)

Approved Signatory

.....End of report.....

Note: 1. Test report shall not be re-produced except in full, without written approval of the laboratory
2. Results related only to the item tested

info@lpilibya.org

المؤسسة الوطنية للنفط
معهد النفط الليبي

TEST REPORT

Issued by : Libyan Petroleum Institute

Date of Issue : 16 / 07 / 2006

Test Report No : 0077/ IL18 /2006

Customer	: Al-Tahadi University
Address	: Sert: P.O.BOX 674
Date sample received	: 10 / 07 / 2006
Sample identification	: soil
Work order No	: 0216 / IL18 / 2006
Sample condition upon receiving	: Good Condition
Testing date	: 16 / 07 / 2006
Customer requested date	: /
Testing venue	: IL18 (AAS & ICP – OES)
Temperature	: 19.9 °C – 20.0 °C
Relative Humidity	: 56 – 58 %RH
Sampling procedure used	: Sample taken by customer on-site
Sampling date	: /
Test Method	: Wet Ash
Testing outcome	: Compliance with the requirement
Measurement uncertainty	: N/A
Opinion and interpretations	: Refer (Table1);

معهد النفط الليبي-طريق قرقارش-7كم ص.ب.6431 ،هاتف 4836021-23 /4830022-27 ، برقية محمور 4830020 / 4830031 بريد الكتروني info@lpilibya.org

Issued by : Libyan Petroleum Institute

Date of Issue : 16 / 07 / 2006

Test Report No : 0077 / IL18 / 2006

Table 1:-

Sample No	Fe ppm
1	1685.2
2	6890.6
3	1664.4
4	918.05
5	8772.6

Abdulgader Elmethnani

Approved Signatory

End of report

Note: 1. Test report shall not be re-produced except in full, without written approval of the laboratory
2. Results related only to the item tested

معهد النفط الليبي طريق قرقارش-7كم ص.ب.6431 ،هاتف 4836821-23 /4836822-27 ، بريد مصور 4830020 / 4830011 بريد الكتروني info@lpilibya.org

معهد النفط الليبي
ادارة بحوث الأستكشاف و المكامن
منسقية المجموعات البحثية
مجموعة الرسوبيات

جامعة التحدي (سرت).

التحاليل المعملية التي أجريت للعينات:

1- التحاليل المنخلية (Sieve analysis).
2- تصنيف المسامية والنفادية (Porosity & Permeability).
3- التركيب الكيميائي (Chemical composition).

أعداد العينات الباحث – محمد سعيد & عبدالله المهدي

Sample(1) weight: 156.6 g

Screen opening (µm)	Weight (g)	Cumulative weight (g)	Weight %	Cumulative weight %
850	3.36	3.36	2.14559387	2.14559387
600	13.21	16.57	8.43550447	10.58109834
425	27.52	44.09	17.5734355	28.15453384
355	14.41	58.5	9.20178799	37.35632184
300	19.33	77.83	12.3435504	49.69987229
212	31.65	109.48	20.210728	69.91060026
180	9.1	118.58	5.8109834	75.72158365
150	9.98	128.56	6.37292465	82.0945083
125	7.81	136.37	4.98722861	87.08173691
90	12.64	149.01	8.0715198	95.15325671
75	3.36	152.37	2.14559387	97.29885057
32	4.1	156.47	2.61813538	99.91698595
25	0	156.47	0	99.91698595

59.3295 FU-ML 59.32% of the sample is between (212-425 µm) which is fine lower to medium lower sand

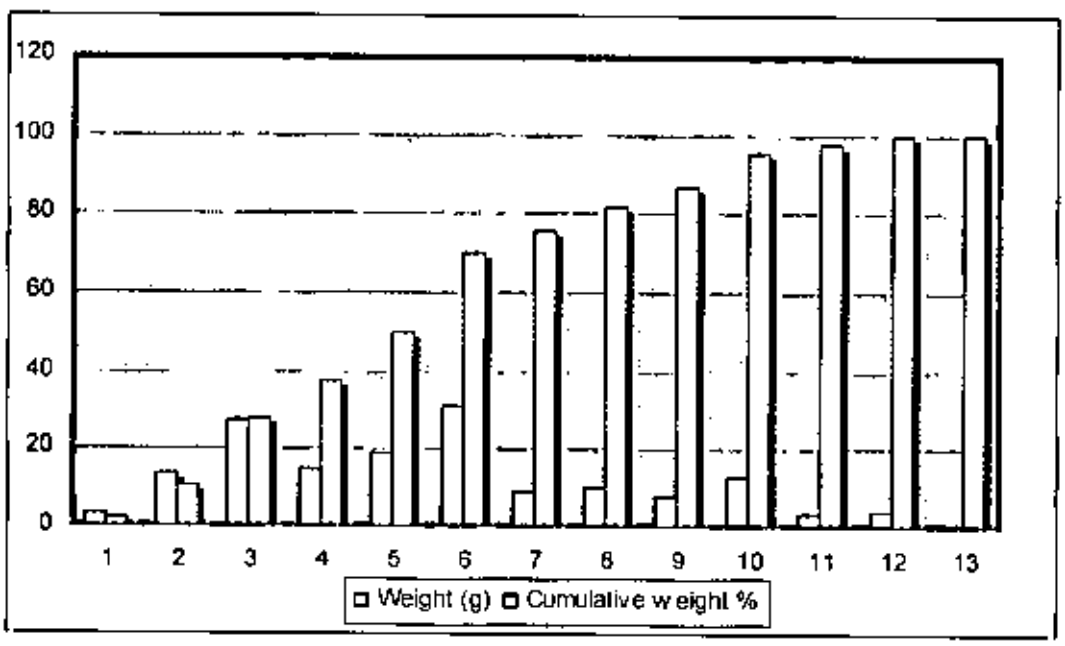

Sample(2)
weight: 58g

Screen opening (µm)	Weight (g)	Cumulative weight (g)	Weight %	Cumulative weight %
850	0	0	0	0
600	0	0	0	0
425	0.1	0.1	0.17241379	0.172413793
355	0.28	0.38	0.48275862	0.655172414
300	0.01	0.39	0.01724138	0.672413793
212	6.31	6.7	10.8793103	11.55172414
180	3.24	9.94	5.5862069	17.13793103
150	5.53	15.47	9.53448276	26.67241379
125	14.1	29.57	24.3103448	50.98275862
90	15.32	44.89	26.4137931	77.39655172
75	4.31	49.2	7.43103448	84.82758621
32	6.68	55.88	11.5172414	96.34482759
25	0.6	56.48	1.03448276	97.37931034

50.72414 VF 50.72% of the sample is between (90-125 µm) which is very fine grained sand

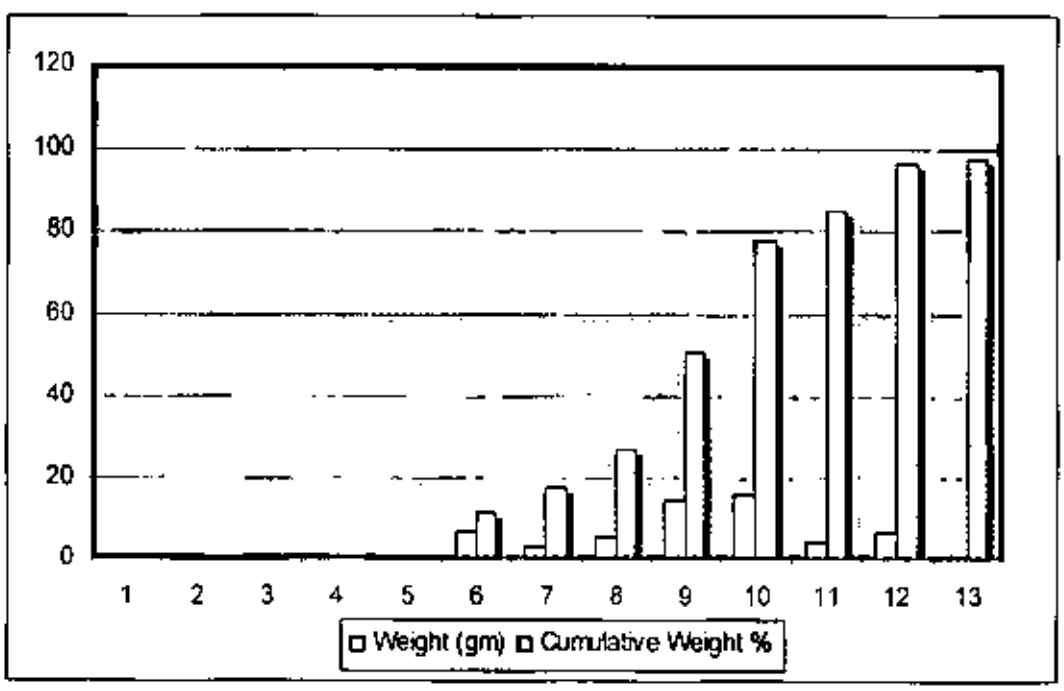

Sample(3)
weight: 264.2g

Screen opening (µm)	Weight (g)	Cumulative weight (g)	Weight %	Cumulative weight %
850	1	1	0.37850114	0.37850114
600	2.23	3.23	0.84405753	1.222558672
425	20.56	23.79	7.78198335	9.004542018
355	26.2	49.99	9.91672975	18.92127177
300	52.46	102.45	19.8561696	38.77744134
212	102.11	204.56	38.6487509	77.42619228
180	20.52	225.08	7.7668433	85.19303558
150	21.44	246.52	8.11506435	93.30809993
125	9.73	256.25	3.68281605	96.99091598
90	6.71	262.96	2.53974262	99.5306586
75	1.06	264.02	0.4012112	99.9318698
32	0.52	264.54	0.19682059	100.1286904
25	0	264.54	0	100.1286904

68.42165 FU-M 68.42% of the sample is between (212-355 µm) which is fine upper to medium grained sand

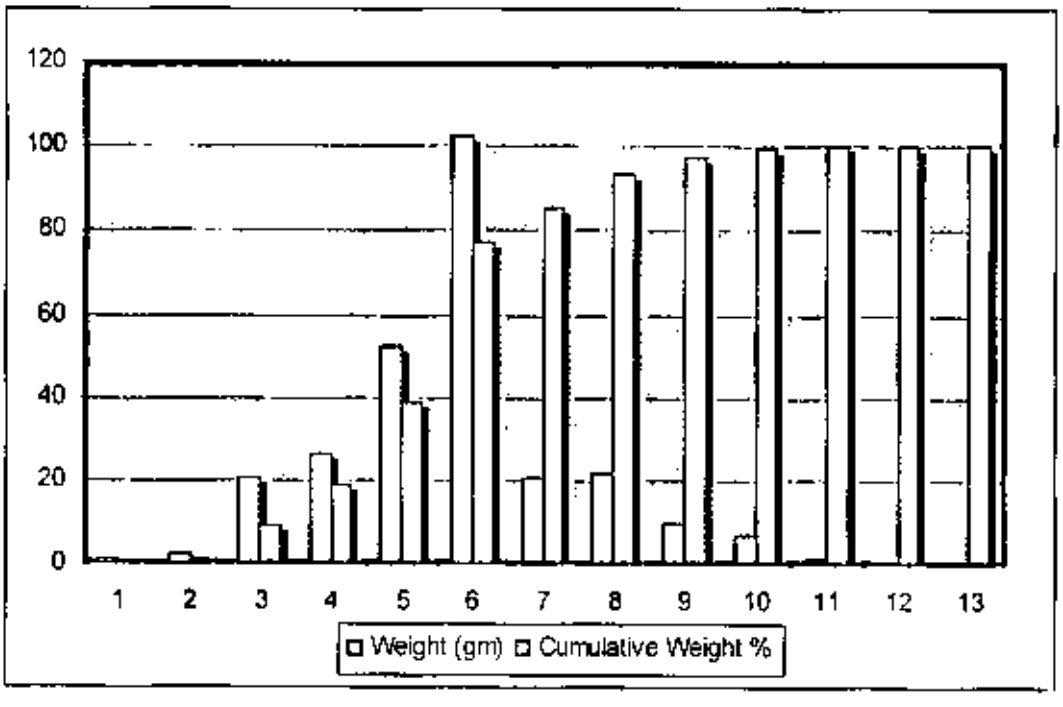

Sample(4) weight: 311.3g

Screen opening (µm)	Weight (g)	Cumulative weight (g)	Weight %	Cumulative weight %
850	6.07	6.07	1.94988757	1.94988757
600	42.91	48.98	13.7841311	15.73401863
425	28.36	77.34	9.1101831	24.84420174
355	27.26	104.6	8.75682621	33.60102795
300	30.26	134.86	9.72052682	43.32155477
212	58.17	193.03	18.6861548	62.00770961
180	23.01	216.04	7.39158368	69.39929329
150	20.29	236.33	6.51782846	75.91712175
125	10.43	246.76	3.35046579	79.26758754
90	5.93	252.69	1.90491487	81.17250241
75	1.3	253.99	0.4176036	81.59010601
32	3.82	257.81	1.22711211	82.81721812
25	51.25	309.06	16.4632188	99.28043688

73.96723 FL-CL 73.96% of the sample is between (150-600 µm) which is fine lower to coarse lower sand

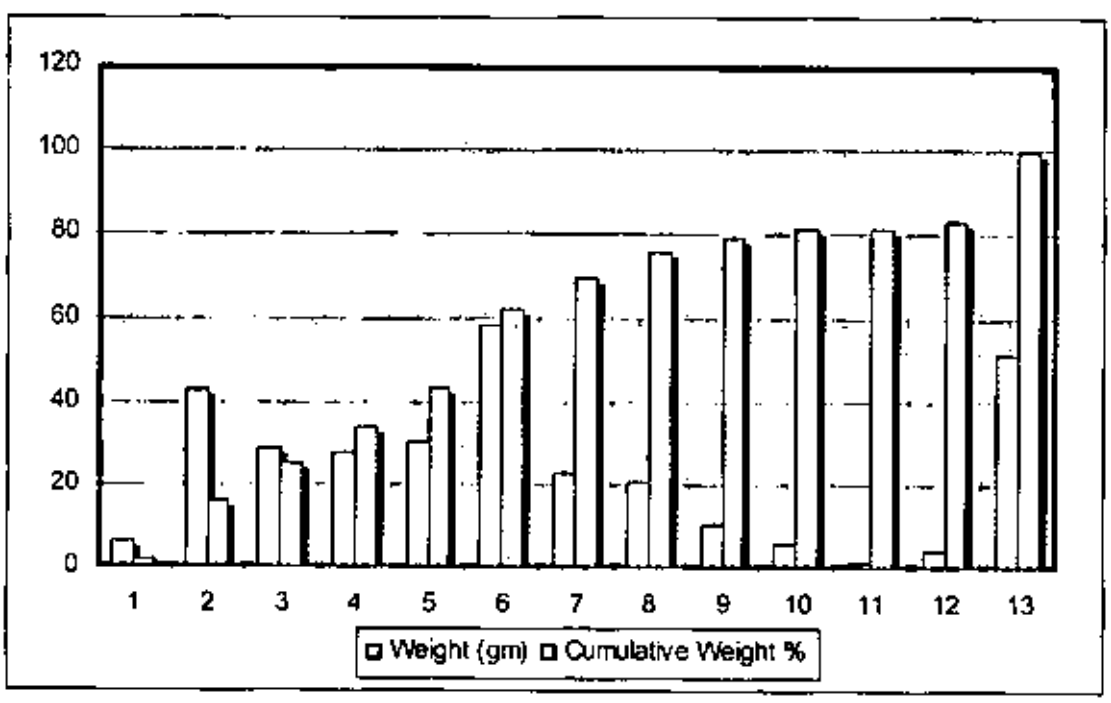

Sample(5)
weight:53.6g

Screen opening (µm)	Weight (g)	Cumulative weight (g)	Weight %	Cumulative weight %
850	0	0	0	0
600	0	0	0	0
425	0.18	0.18	0.3358209	0.335820896
355	0.11	0.29	0.20522388	0.541044776
300	0.22	0.51	0.41044776	0.951492537
212	1	1.51	1.86567164	2.817164179
180	0.78	2.29	1.45522388	4.27238806
150	1.73	4.02	3.22761194	7.5
125	3.24	7.26	6.04477612	13.54477612
90	16.94	24.2	31.6044776	45.14925373
75	8.71	32.91	16.25	61.39925373
32	19.55	52.46	36.4738806	97.87313433
25	1.15	53.61	2.14552239	100.0186567

84.32836 SLT-VF 84.32% of the sample is between (32-90 µm) which is silt to very fine sand

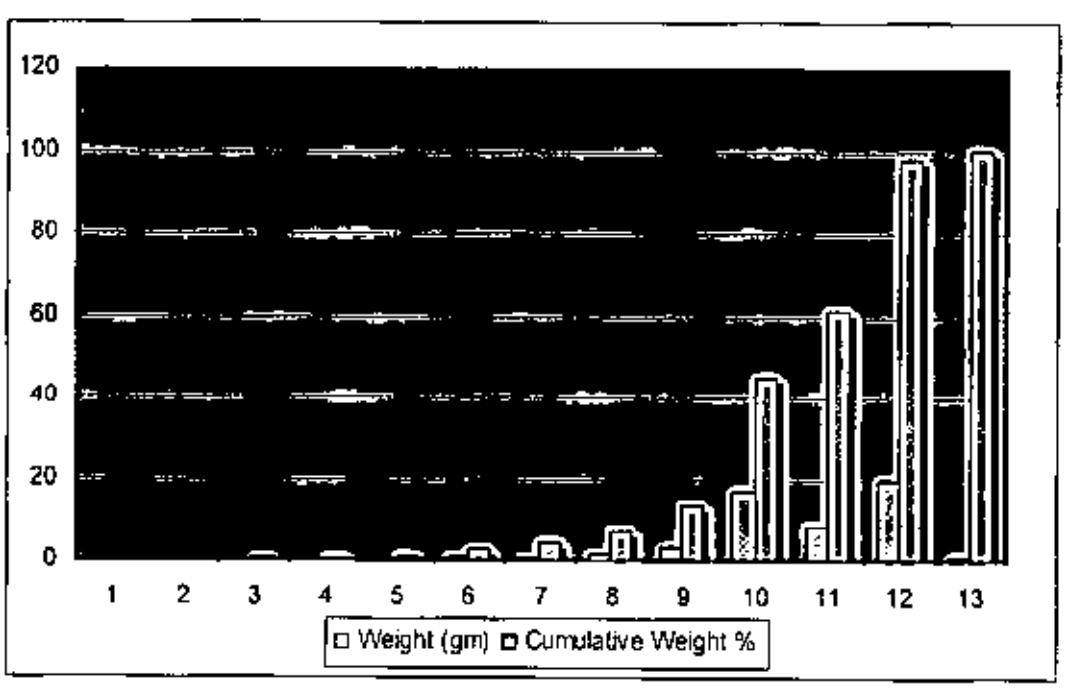

Approximate values of porosity hydraulic conductivity for various aquifers (from Domenico and Schwarz, 1990, Physical and Chemical Hydrogeology, John Wiley & Sons, New York,

Sample No-	*Grain size range (classification)*	Porosity (%)	*Hydraulic Conductivity (ft/sec)*
1	*(90-125 μm) very fine grained sand*	26——53%	6.0×10^{-7} - 6.0×10^{-4}
2	*(90-125 μm) very fine grained sand*	26——53%	6.0×10^{-7} - 6.0×10^{-4}
3	*(212-355 μm) fine upper to medium grained sand*	34——61%	3.0×10^{-9} - 6.0×10^{-5}
4	*(150-600 μm) fine lower to coarse lower sand*	34——61%	3.0×10^{-9} - 6.0×10^{-5}
5	*(32-90 μm) silt to very fine sand*	34——61%	3.0×10^{-9} - 6.0×10^{-5}

Characteristics affecting Hydraulic conductivity and Porosity

Appendix (B)

B1 Program (1) :

```
% This Program for Calculate the Dielectric Constant
% S=SiO2 , A = Al2O3 , F = Fe2O3 ,C = CaCO3 , M = MgCO3 .
('S=SiO2 , A=Al2O3 , F=Fe2O3 ,C=CaCO3 , M=MgCO3')
X= input ('what the name of element "S,A,F,C,M"=','S');

S = sym('S');
A = sym('A');
F = sym('F');
C = sym('C');
M = sym('M');

if X == S
     V1 = input('V=');
Si=4.43-0.04i;
S=Si^(1/3);
    Diel =S*V1
else if X == A
          V2 = input('V=');
Al=12.66-1.31i;
A=Al^(1/3);
    Diel=A*V2
    else if X == F
             V3 = input('V=');
Fe=16.58-0.93i;
F=Fe^(1/3);
    Diel=F*V3
        else if X == C
          V4 = input('V=');
Ca=5.01-0.08i;
C=Ca^(1/3);
    Diel=C*V4
             else if X == M
          V5 = input('V=');
Mg=5.03-0.17i;
M=Mg^(1/3);
    Diel=M*V5
                 else
                 ('Sorry; this element not presents')
                 end
            end
        end
    end
end
```

Run Program:

```
<<diel

ans=

S=SiO2 , A=Al2O3 , F=Fe2O3 ,C=CaCO3 , M=MgCO3

what the name of element "S,A,F,C,M"=S
V=0.903

diel=

1.4831 – 0.0045i

<<diel

ans=

S=SiO2 , A=Al2O3 , F=Fe2O3 ,C=CaCO3 , M=MgCO3

what the name of element "S,A,F,C,M"=N

ans=

Sorry; this element not presents
```

B2 Program (2) :

```
% This Program for Particle-Size Distribution Cumulative
%  ( analysis samples from factory of steel iron )

y=[.10 .15 .4 .6 .85 1.2];
x1=[51.28 44.43 2.81 1.05 0.23 .2];
x2=[16.91 56.8 14.83 8.97 2.31 .18];
plot (y,x1)
hold on
grid
plot (y,x2,'r')
xlabel('Particle Diameter (mm)')
ylabel('Weight (g)')
```

Run Program:

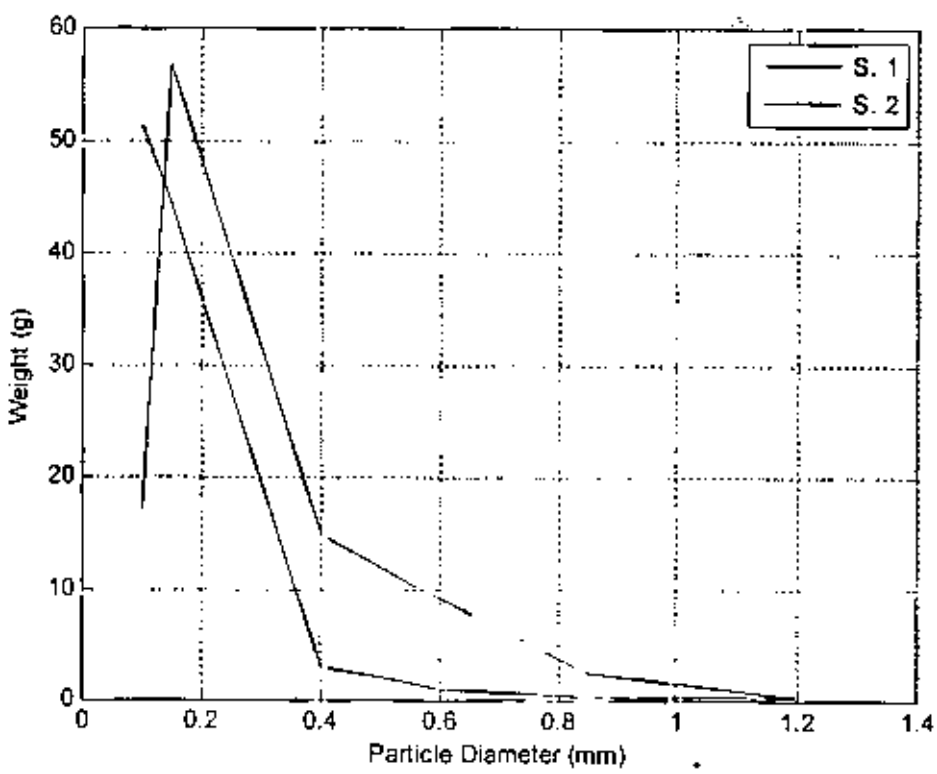

B3 Program (3) :

```
% This program for Particle-Size Distribution Cumulative
%  ( analysis samples from Center of  petroleum study )

y=[850 600 425 355 300 212 180 150 125 90 75 32 25];
x1=[3.36 13.21 27.52 14.41 19.33 31.65 9.1 9.98 7.81 12.64
3.36 4.1 0.0];
x11 =x1/1.566;
s1=sum(x1);
s1=s1/13;

x2 =[0.0 0.0 0.1 0.28 1.01 6.31 3.24 5.53 14.1 15.32 4.31
6.68 0.6];
x22 = x2/0.58;

x3 =[1 2.23 20.65 26.2 52.46 102.11 20.52 21.44 9.73 6.71
1.06 0.52 0.0];
x33=x3/2.642;

x4 =[6.07 42.91 82.36 27.26 30.26 58.17 23.01 20.29 10.43
5.93 1.3 3.82 0.25];
x44=x4/3.113;

x5=[0.0 0.0 0.18 0.11 0.22 1.0 0.78 1.73 3.24 16.94 8.71
19.55 1.15];
x55=x5/0.536;

plot (y,x11);
hold on
grid
plot (y,x22,'r');
plot (y,x33,'m');
plot (y,x44,'c');
plot (y,x55,'G');
xlabel('Particle Diameter (μm)')
ylabel('Weight (g)')
```

Run Program:

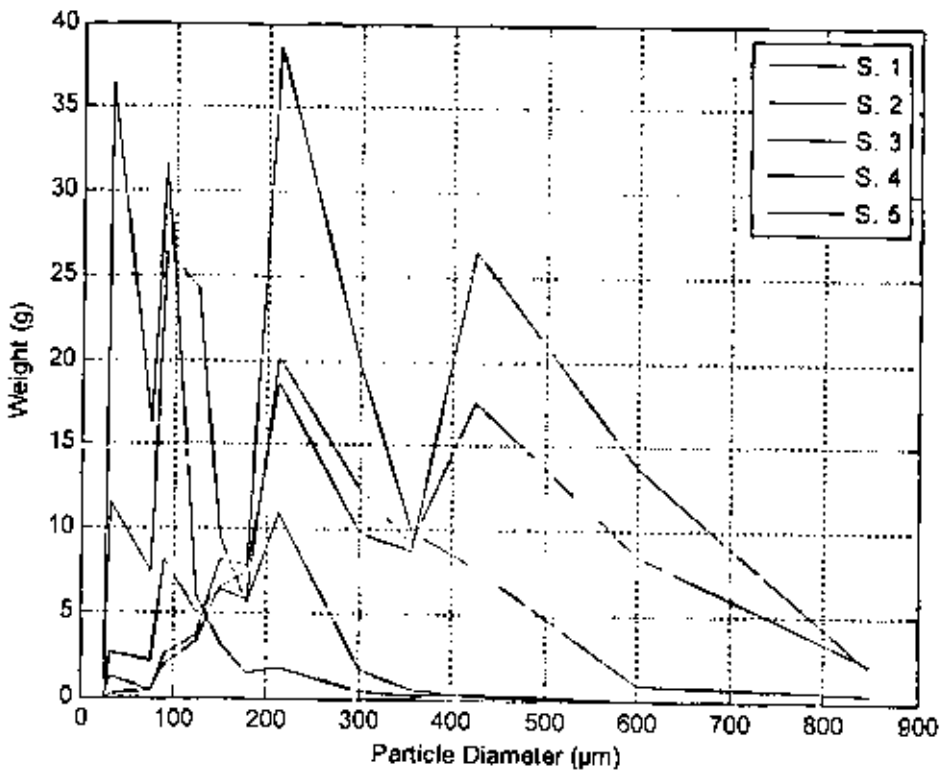
S. 1
S. 2
S. 3
S. 4
S. 5
Weight (g)
Particle Diameter (µm)
0
5
10
15
20
25
30
35
40
0
100
200
300
400
500
600
700
800
900

B4 Program (4) :

```
% This Program for Calculate the Visibility
% (from Maximum wind speed in station in Jalo and Agedabia)

('How many the number of wind speed input')
N= input ('N=');
K = 3000 ;
('Input the  max. wind speed')
for T = 1:N
    A(1,T) = input ('S = ');

end
for T = 1:N
   S(T)=A(1,T);
  B=S(T);
   V(T) = (K/B);

end
S(T)=S(T)
V(T)=V(T)
```

Run Program:

```
How many the number of wind speed input
N=14

ans =
Input the  max. wind speed
S = 19
S = 23
S = 20
S = 18
S = 15
S = 18
S = 20
S = 24
S = 20
S = 20
S = 20
S = 30
S = 20
S = 18

S =
18   20   30   20   20   20   24   20   18   15   18   20   23   19

V =
Columns 1 through 9
125.0000  150.0000  166.6667  200.0000  166.6667  150.0000  130.4348  157.8947
150.0000
Columns 10 through 14
166.6667  150.0000  100.0000  150.0000  150.0000
```

B5 Program (5) :

```
% This Program Calculate the Attenuation Coefficient
% (Method 1)


('Input the  Frequency (Ghz)')
F= input ('F= ');
('Input the dielectric constant ')
a1=input ('abs1= ');
a2=input ('abs2= ');
('Input the number of Visibility input')
N = input('N= ');
('Input the  Visibility (km)')
for T = 1:N
    C(1,T) = input ('V = ');
end
L=3/(F*10);
e =0.000075;
Ae=e/L;
K1=((a1+2)^2)+a2^2;
K2=3*a2;
K=K2/K1;
for T = 1:N
W = C(1,T);
    M=189/W;
    A(1,T)=M*Ae*K;
      V(T)=C(1,T);
   Att(T) = A(1,T);

x(T)=V(T);
y(T)=Att(T);
end

V(T)=V(T) ;
Att(T)=Att(T)

plot (x,y)
hold on
grid
xlabel('Visibility (km)')
ylabel('Attenuation (dB)')
```

Run Program:

```
Input the  Frequency (Ghz)

F= 3

ans =

Input the dielectric constant

abs1= 4.9871
abs2= 0.08195

ans =

Input the number of Visibility input

N= 10

ans =

Input the  Visibility (km)

V = 0.10021
V = 0.10865
V = 0.11088
V = 0.12018
V = 0.12231
V = 0.12348
V = 0.12773
V = 0.14221
V = 0.16111
V = 0.17735


Att =

  Columns 1 through 6

    0.0071    0.0066    0.0064    0.0059    0.0058
0.0058

  Columns 7 through 10

    0.0056    0.0050    0.0044    0.0040
```

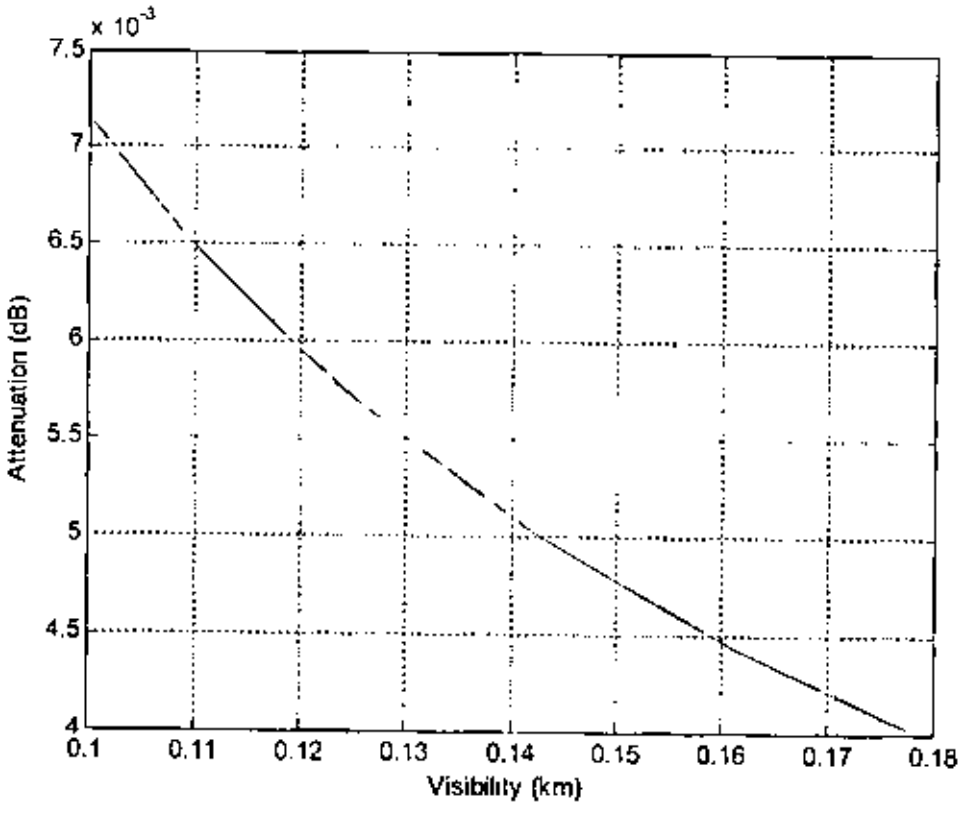
x 10^-3
7.5
7
6.5
6
5.5
5
4.5
4
Attenuation (dB)
0.1
0.11
0.12
0.13
0.14
0.15
0.16
0.17
0.18
Visibility (km)

B6 Program (6) :

```
% This Program for Calculate the Attenuation (Method 2)
% D= the path length in the storm (Km)(1,5,10,20 Km)
% L= wavelength in 10Ghz (3cm)
% V = visibilty (Km)

%D= input ('D')
%L = input('L')
('Input the  Frequency (Ghz)')
F= input ('F= ');
('Input the dielectric constant ')
a1=input ('abs1= ');
a2=input ('abs2= ');
('Input the number of Visibility input')
N = input('N= ');
('Input the  Visibility (km)')
for T = 1:N
    C(1,T) = input ('V = ');
end
L=3/(F*10)
A2=(((a1+2)^2)+ a2^2)*L
for T = 1:N
W = C(1,T);
V1=W^1.07
v=(1.5265E-8)/V1
A1=(2.46*v*a2)*10E5

A(1,T)=A1/A2

      V(T)=C(1,T);
   Att(T) = A(1,T);

x(T)=V(T);
y(T)=Att(T);
end

V(T)=V(T) ;
Att(T)=Att(T)

plot (x,y)
hold on
grid
xlabel('Visibility (km)')
ylabel('Attenuation (dB)')
```

Run Program:

Input the Frequency (Ghz)

F= 3

ans =

Input the dielectric constant

abs1= 4.71965
abs2= 0.08195

ans =

Input the number of Visibility input

N= 10

ans =

Input the Visibility (km)

V = 0.10021
V = 0.10865
V = 0.11088
V = 0.12018
V = 0.12231
V = 0.12348
V = 0.12773
V = 0.14221
V = 0.16111
V = 0.17735

Att =

Columns 1 through 6

0.0080 0.0073 0.0072 0.0066 0.0065 0.0064

Columns 7 through 10

0.0062 0.0055 0.0048 0.0043

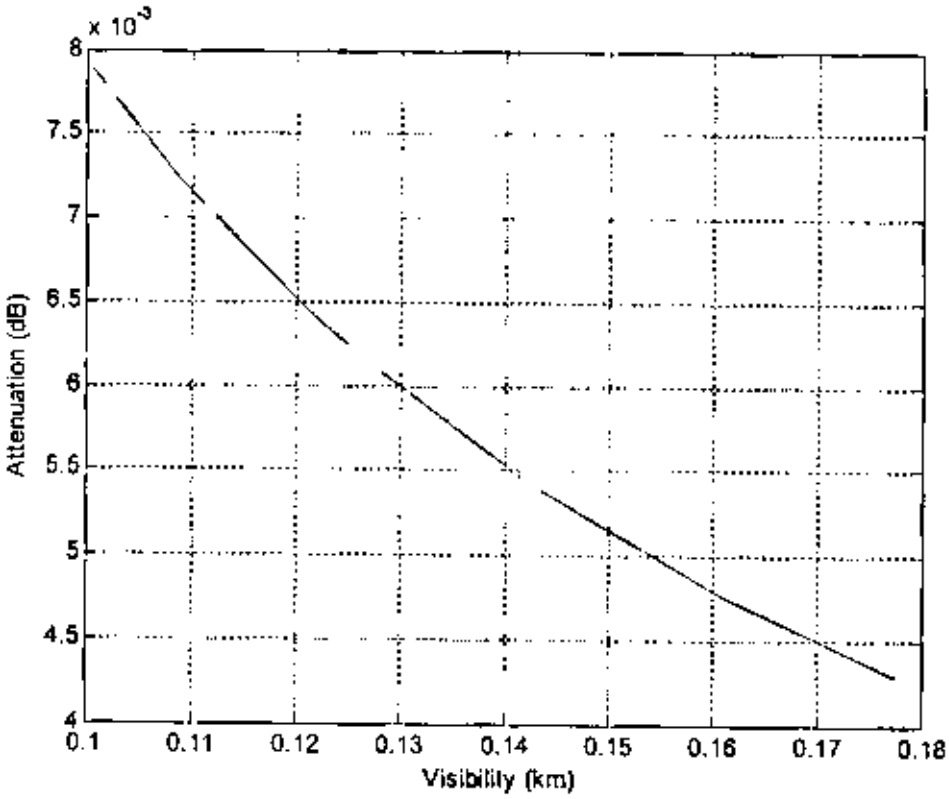
x 10^-3
8
7.5
7
6.5
6
5.5
5
4.5
4
Attenuation (dB)
0.1
0.11
0.12
0.13
0.14
0.15
0.16
0.17
0.18
Visibility (km)